EFFECTS OF PROCESSING PARAMETERS AND THICKNESS ON COMPRESSION-MOLDED PET/GF COMPOSITES

A Thesis
Submitted to the Graduate Faculty
of the
North Dakota State University
of Agriculture and Applied Science

By

Jacob Aaron Reinholz

In Partial Fulfillment of the Requirements
for the Degree of
MASTER OF SCIENCE

Department:
Mechanical Engineering

April 2024

Fargo, North Dakota

North Dakota State University
Graduate School

Title

EFFECTS OF PROCESSING PARAMETERS AND THICKNESS ON COMPRESSION-MOLDED PET/GF COMPOSITES

By

Jacob Aaron Reinholz

The Supervisory Committee certifies that this ***disquisition*** complies with North Dakota State University's regulations and meets the accepted standards for the degree of

MASTER OF SCIENCE

SUPERVISORY COMMITTEE:

Dr. Chad Ulven
Chair

Dr. Long Jiang

Dr. Dean Webster

Approved:

April 12th, 2024
Date

Dr. Chad Ulven
Department Chair

ABSTRACT

Polymer-matrix composites (PMCs) have become an integral material in many industries due to excellent strength-to-weight ratio and low cost. When semi-crystalline polymer thermoplastics, such as polyethylene terephthalate (PET), are heated past their melt temperature then cooled during compression molding, the long polymer chains in the amorphous regions unravel and align to form crystalline regions with improved strength and stiffness. This research aimed to understand the effect of compression molding processing parameters such as temperature, pressure, dwell, and cooling rate as well as the overall panel thickness on crystallinity and mechanical properties of unidirectional glass fiber-reinforced PET. It was found that a slower cooling rate and a slightly increased dwell time had the most significant effect on PMC properties. Additionally, uniform crystallinity and scattered mechanical property data taken from specimens throughout thick-section samples suggests there was no symmetric property gradient through the cross-section that affected material performance.

ACKNOWLEDGMENTS

I want to extend a deep gratitude to Dr. Chad Ulven, the committee chair and mentor of this research project. We have worked together for many years, and I have learned so much during this time under his guidance. I would also like to thank Dr. Dean Webster and Dr. Long Jiang for dedicating time out of their busy schedules to serve on my committee and provide key insights into the world of polymer science. I also owe a huge thank you to Luke Gibbon as he was involved in every step of this research and without his devotion and availability to assist, this project would not be nearly as complete. I would also like to thank the Ground Vehicle Systems Center and the National Center for Manufacturing Sciences for sponsoring this research. Lastly, I would like to thank the following individuals for their help in both big ways and small: Rob Sailer, Francisco Valenzuela, Greg Strommen, Eric Hall, Tanya Erickson, Kimberly Carlson, Elizabeth Brouillard, Curt Doetkott, Evan Rasset, Jena Marcolena, Avery Jorgenson, Jacob Sundberg, Evan Reinholz, Anna Reinholz, and Seth Herner.

TABLE OF CONTENTS

LIST OF TABLES

LIST OF FIGURES

LIST OF EQUATIONS

LIST OF ABBREVIATIONS

ABS.....Acrylonitrile butadiene styrene

ASTM .....American Society for Testing and Materials.

ANOVA .....Analysis of variance

CF.....Carbon fiber

CM .....Compression modulus

CS.....Compression strength

CAD .....Computer aided design

DSC.....Differential scanning calorimetry

Eq .....Equation

FEA .....Finite element analysis

GF .....Glass fiber

ILSS .....Interlaminar shear strength

Tm .....Melt temperature

PPT.....Peak processing temperature

PEEK.....Polyether ether ketone

PET .....Polyethylene terephthalate

PMC .....Polymer matrix composite

PP .....Polypropylene

TM.....Tensile modulus

TS .....Tensile strength

TGA .....Thermogravimetric analysis

LIST OF APPENDIX FIGURES

1. INTRODUCTION

In recent years, polymer-matrix composites (PMCs) have gradually replaced metals in numerous industries such as aerospace, marine, and automotive [1]. The latest Global Automotive Composites Market report states that PMCs footprint on the industry is projected to grow from $5.4 billion in 2020 to $9.3 billion by 2025 [2]. As vehicle manufacturers aim to design a lightweight body that still possesses exceptional strength, PMCs prove to be the superior engineering material for these applications. Continuous fiber composites are one subset of PMCs, in which a long reinforcing fiber, such as carbon or glass, is surrounded by a polymer matrix. The strength and stiffness of the fiber is used to enhance the overall properties of the composite. Thermoplastics have been increasingly preferred over thermosets as a polymer matrix due to the indefinite shelf-life, short processing time, and recyclability [3]. The reusable nature of thermoplastics stems from their ability to undergo several heating and cooling cycles, whereas thermosets can only be cured once. Pre-impregnated composites, or “prepregs” are fiber sheets that are intertwined with cured thermoplastic resin [4]. These sheets can then be manipulated and processed to achieve the desired composite part.

The diverse manufacturability of PMCs allows parts to be fabricated in any size or shape, and the fibers can also be aligned to optimize performance. Compression molding is a popular technique used to fabricate PMCs. A hydraulic press is used to compress the composite material into a custom mold while heated platens raise the temperature past the melting point of the thermoplastic. The thermoplastic then flows freely inside the mold before the heat is removed and the composite solidifies into a laminate. Most laminates produced in the automotive industry are thin section parts designed for a vehicle’s exterior door panels, hood, and fenders [2]. Because the relationship between composite thickness and mechanical properties is largely

unknown, PMCs are not used for structural applications requiring thick section laminates. In addition to part thickness, changes in the processing parameters used during compression molding will alter the overall properties as well. These parameters include pressure, temperature, dwell time, and cooling rate. This research aims to understand the effect of processing parameters and laminate thickness on PMC properties.

This thesis is composed of eight sections. Firstly, the introduction will summarize background information on material selection and previous research into thick-section PMCs and subsequent processing parameters. The second section defines objectives for this research which includes the effect of laminate thickness and processing parameters on composite material properties such as crystallinity and mechanical strength and modulus. Third, the methodology used to conduct this study will be described. This includes a test matrix of laminate thicknesses and processing parameters that, when completed, will illustrate a thorough but efficient method of achieving the objectives. Additionally, this section will show all equipment and fixtures used in the manufacturing, cutting, and testing of composite specimens. The fourth section reports the results of this research including the analysis of variance (ANOVA). The fifth and sixth sections discuss the findings of the study in relation to the hypotheses developed during the literature review and offer recommendations into future research into this area. Lastly, the seventh and eighth sections include the references and appendix.

1.1. Material Selection

1.1.1. Fiber Orientation

The method in which the fiber reinforcement material is added to a polymer matrix has a significant effect on composite properties. The two main groups of fiber reinforcement are continuous, or long fiber, and discontinuous, or short fiber. This research focused on continuous

fiber which can be further categorized into unidirectional or multiaxial as shown in Figure 1. In unidirectional PMCs, the fiber is oriented in a single direction, whereas in multiaxial PMCs, the fiber can be woven into multiple directions (most commonly a biaxial weave) to create a commingled single ply, or individual plies of unidirectional fiber can be stacked in several directions in cross-ply fashion.

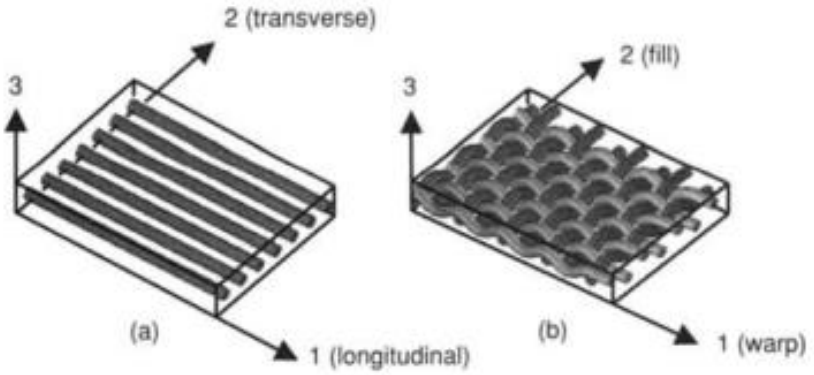

Figure 1. Unidirectional and multiaxial fiber orientation [4]

1.1.2. Fiber Material

In addition to fiber orientation, fiber material is also very important. PMCs used in industry mostly consist of carbon fiber (CF) and glass fiber (GF) [5]. While CF may have higher strength and stiffness at a lighter weight, it is very expensive. Additionally, the coefficient of thermal expansion of CF is negative, meaning that it expands while cooling [6]. When bonded with a contracting polymer matrix during compression molding, this may lead to increased stress concentrations throughout the cured composite. Meanwhile, the extraordinarily low cost of GF for its given strength is unmatched and provides a plethora of other desirable properties including excellent corrosion resistance and great manufacturability across a wide range of processes. Thus, GF is the most widely used fiber reinforcement throughout composite industries [7]. One potential drawback of GF, specifically in thick-section composites, is its low thermal conductivity [8]. This insulative property prevents heat from rapidly propagating through the

thickness of a part. As a result, this could have a significant impact on properties within different sections of a thick composite from a thermodynamic standpoint.

1.1.3. Polymer Material

Like the fiber reinforcement material, the polymer matrix material is also a factor in composite processing and performance. Depending on the application, polymer options range from low-cost commodity plastics to expensive high-performance plastics. According to Markarian, polypropylene (PP) is estimated to occupy roughly 65% of the long fiber thermoplastic market, specifically in the automotive industry, while midlevel engineering polymers such as polyethylene terephthalate (PET) and acrylonitrile butadiene styrene (ABS) account for approximately 15% [9].

One characteristic of thermoplastic polymers that must be considered when selecting a matrix material is crystallinity. The microstructure of thermoplastics can be divided into two categories: amorphous and crystalline. The atoms within amorphous regions are arranged in a random, disordered fashion whereas in crystalline regions, these atoms are aligned into highly ordered, repeating three-dimensional lattice structures. Due to their compact, high-density orientation, crystalline regions have a greater resistance to dislocation motion, or the abrupt rearrangement of atoms, and thus contain increased strength and modulus compared to amorphous regions. The ratio of crystalline regions to total polymer within a sample is called crystallinity and is represented as a percentage. For this research, PET was chosen as the matrix polymer because its semi-crystalline composition was a property of special interest as it is desired to better understand the processing effects on crystallinity and overall performance. Although 100% crystallinity is unattainable in PET, it was hypothesized that adjusting the processing parameters to maximize this value would increase the mechanical properties [10].

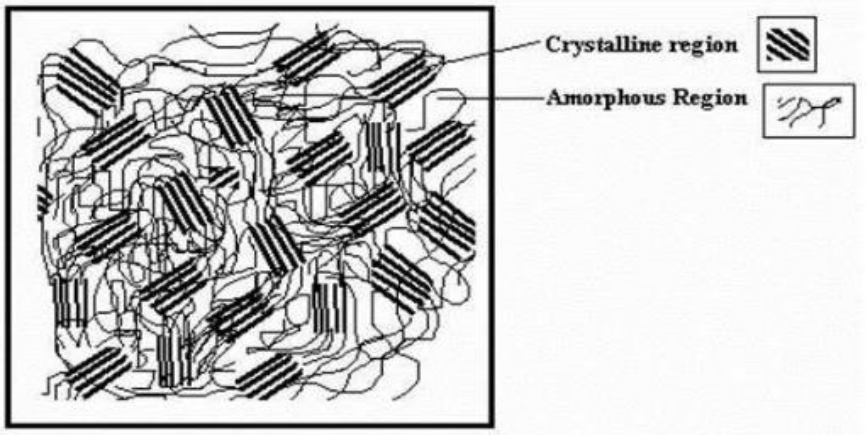

Figure 2. Crystalline and amorphous regions in thermoplastics [4]

1.2. Compression Molding

Compression molding is widely used in the processing of continuous fiber PMCs, specifically those used in large, simply shaped parts. Rolls of prepreg fabric can easily be trimmed into sheets and stacked within a mold. Two platens are compressed using hydraulic cylinders as heat is conducted through the platens into the mold as shown in Figure 3. Many compression presses have the capabilities to adjust temperature and pressure both manually and automatically. These features are especially helpful when customizing certain compression molding recipes.

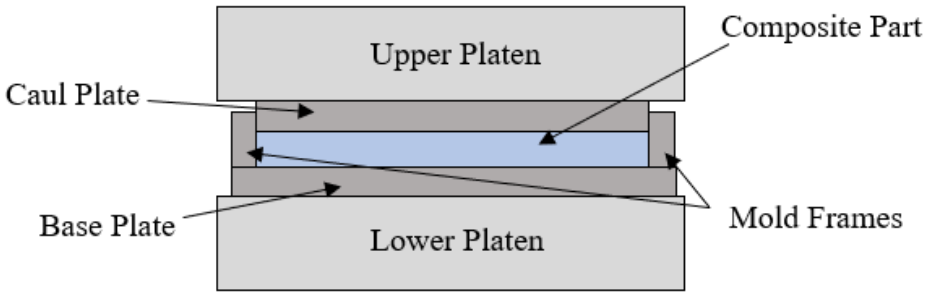

Figure 3. Compression mold diagram

1.3. Processing Parameters

1.3.1. Peak Processing Temperature

Peak processing temperature (PPT) is the maximum temperature to which the composite is heated during the compression molding process. PMC manufacturers typically provide a recommended PPT range of roughly 32-100°F above the melt temperature of the polymer. Studies have reported that adjusting the PPT can have a significant effect on overall properties. Jar et al. showed that increasing the PPT by roughly 70°F above recommended temperature increased the tensile properties in 45° and 90° polyether ether ketone (PEEK)/CF specimens due to improved interfacial adhesion [11]. Ye et al. found that at a constant pressure, the best consolidation of PEEK/CF composites was at nearly 210°F above the melt temperature of the polymer [12]. Similarly, Bernhardsson and Shishoo showed an 80% increase in tensile strength, by increasing the processing temperature of PP/GF from 338°F to 428°F [13]. While increasing the PPT may improve properties, researchers must be careful not to surpass the degradation temperature at which the individual monomers in the polymer begin to separate from the chain. One study investigating PET nanocomposites suggested that degradation begins around 660°F [14].

1.3.2. Pressure

The pressure applied to the composite is most likely to affect the void content. A lower processing pressure may allow sufficient matrix flow but could risk excessive air pockets to remain embedded within the composite. Thus, a higher pressure is recommended to prevent voids which are detrimental to material properties [15]. One study investigating the effect of processing pressure on mechanical properties in PET/GF composites found a near linear increase in tensile strength and modulus over a pressure range of 0.10 to 0.41 ksi [16]. The study also

showed insignificant to slightly negative effects on flexural strength and modulus over the same range.

1.3.3. Dwell

Dwell, or holding time, is the time spent at the peak processing temperature and pressure before the cooling stage is initiated. As the thermoplastic is heated past its melt temperature, T_m, the crystalline regions transition to amorphous as the polymer decreases its viscosity and begins to flow. An important factor in the processing of PMCs is the consolidation level which requires an even distribution of matrix material throughout the fibers. This is accomplished by providing the polymer sufficient time above the T_m to completely wet out the fibers. Thus, the effects of dwell are of great interest. Wakeman et al. suggests that holding time need not exceed 1 min to achieve full consolidation whereas other studies recommend upwards of 20 min [12], [17], [18]. At holding times over 20 min, the polymer may be at risk of degradation which will negatively affect composite performance [19]. An alternate option to avoid this consequence is to heat the composite well above the glass transition temperature, T_g, but below the T_m, and increase the applied pressure from the platens to force polymer flow at a lower viscosity.

1.3.4. Cooling Rate

After the composite is heated past the polymer's T_m and the thermoplastic completely wets out the GF, the panel must cool to room temperature. Since the polymer chains require time to realign into crystalline form, it follows that a prolonged duration at high temperature will promote this phenomenon. Like the annealing or quenching process used in the heat treatment of metals, the rate of cooling can significantly alter the composite properties by changing the microstructure of the material. Wang et al. compared a gradual cooling rate under 2.5 MPa of pressure within a hot press and a rapid cooling rate under normal ambient conditions [18]. This

study showed six times greater void content and a 23.4% decrease in tensile strength in the ambient cooling compared with the gradual cooling conditions. Gauthier et al. found that decreasing the cooling rate 90°F/min to 14.4°F/min improved the crystallinity in unidirectional glass/PET from 20% to 30% [20]. It may prove difficult to determine an optimal cooling rate due to the fact that the crystallization rates vary with changing temperature. Research suggests the quickest crystallization rate of PET occurs between 338°F-374°F so a recipe with a dwell period in this range may prove to be beneficial [10], [21].

1.3.5. Laminate Thickness

One motivation of this research is to better understand how the properties of the compression molded composite translate into thicker sections while in the presence of high fiber content. This knowledge is key in obtaining the ability to model PET/GF in CAD software over a variety of thicknesses. Polymer crystallinity is the predominate factor in differing properties through the composite thickness. During the cooling stage, the outer layers of the composite cool faster than the inner layers, resulting in a crystallinity gradient throughout the thickness of the laminate. It is hypothesized that the percent crystallinity will roughly resemble that shown in Figure 4. The maximum crystallinity of semi-crystalline PET is largely unknown; however, Charrier suggests PET can reach a percent crystallinity of 30% under ideal processing conditions [22]. This research will utilize PET that is already semi-crystalline prior to compression molding, so the post-processing crystallinity is expected to be greater than 30%.

Figure 4. Hypothesized PET percent crystallinity throughout panel thickness

2. OBJECTIVES

Before a material can be implemented in a vehicle component, two preliminary tasks in the pre-production stage must be accomplished. First, a manufacturing process must be defined that will produce the desired component shape and match the material's natural properties with the application. Second, the material must be modeled using finite element analysis (FEA) software to understand how it responds to certain loading scenarios. Common vehicle metals such as steel and aluminum are well researched and can provide accurate responses to loadings based on known properties. Contrarily, composite materials such PET/GF have limited amounts of research and are largely unpredictable in modeling, especially when attempting to understand the crystallinity effects in thick-section composites. Data received from this research will help determine an optimal compression molding process and provide information needed to create accurate FEA models for PET/GF components. The following research objectives have been identified to accomplish these tasks:

- Evaluate the effects of PPT, pressure, dwell, and cooling rate on composite properties
- Evaluate the effects of laminate thickness on composite properties

Many sources have researched the effects of these variables on similar composite materials, as summarized in Section 1.3. From this literature review, it is hypothesized that material performance will increase with PPT and holding time up to a certain value at which polymer degradation will initiate. Increased pressure is expected to improve properties while the slowest cooling rate tested is likely to deliver the highest crystallinity and laminate performance. In the laminate thickness study, the percent crystallinity is expected to mimic the illustration in Figure 4. Composite properties include strength and elastic modulus in tension, compression, and shear as well as percent crystallinity as outlined in Table 1.

Table 1. Summary of material properties and corresponding test standards

Property	ASTM
Tensile	D3039
-Strength (90°)	
-Modulus (0°)	
Compression	D695
-Strength (0°/90°)	
-Modulus (0°/90°)	
Interlaminar Shear	D2344
-Strength	
Crystallinity	D3418

3. RESEARCH METHODOLOGY

3.1. Material

The material of study was Toray Cetex TC940 PET/GF produced by Toray Advanced Composites. It is a low-cost unidirectional prepreg thermoplastic composite tape that has excellent strength and modulus in the longitudinal direction as shown inTable 2. This formulation has a density of 1.89 g/cm^3 and fiber fraction of 60% by weight with a recommended processing temperature of 490-530°F [23]. Cetex TC940 is advertised to be used primarily in sporting goods and automotive styling applications. It was also noted to be black in color compared to standard PET that typically has a white or clear appearance as seen in Figure 5. This is likely due to a pigment additive such as carbon black included in the formulation.

Table 2. Mechanical properties of Toray Cetex TC940

Property	ASTM Standard	Typical Results
Tensile Strength/Modulus (0°)	D3039	139 ksi/4.6 Msi
Flexural Strength/Modulus (0°)	D790	176 ksi/4.7 Msi
Compressive Strength (0°)	D3410	48 ksi
Interlaminar Shear Strength	D2344	5.9 ksi

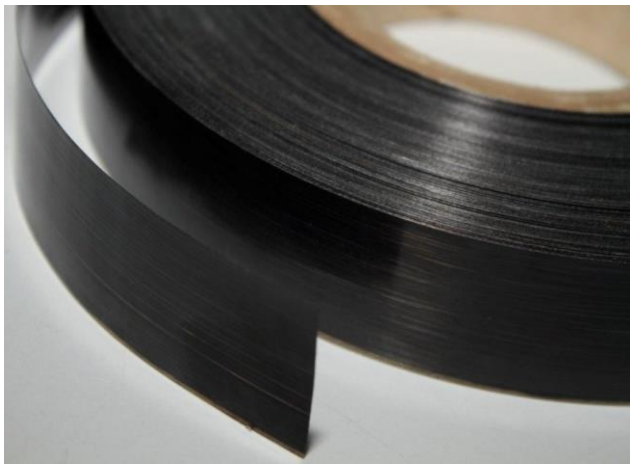

Figure 5. Toray Cetex TC940 PET unidirectional tape [24]

3.2. Processing Apparatus

3.2.1. Compression Press

The processing machine used in this research was a Wabash Genesis G30H-24 30-ton compression press (see Figure 6). The platens were 24 in *x* 24 in with heat capabilities up to 650°F and included air and water-cooling features. Customized recipes could be programmed into the press to allow semi-automatic cycling of process conditions. Early testing of the press capabilities suggested that the material temperature inside the mold lagged the preset cooling rate by varying amounts. Thus, the cooling rate was set at 6.5, 13.5, and 22.5°F/min for the actual 5, 12.5 and 20°F/min cooling rates planned. For the 1 in and 2 in panels, set points of 14.5 and 15.5°F/min were used to achieve the 12.5°F/min cooling rate.

Figure 6. Wabash Genesis four-post compression press [25]

3.2.2. Mold

Three iterations of molds were used to complete the objectives of this study. Each was a matched tool mold design with dimensions that best suit the pre-processed material size. The mold cavity was formed by a supporting base plate, two pairs of surrounding frame rails, and a top caul plate. A cavity length of 22 in was chosen to maximize the size of specimens produced per cycle for the specified platen dimensions. A cavity width of 6.6 in was chosen to accommodate the 6.5 in width of the unidirectional tape. The dimensions of each mold iteration are listed in Table 3. 6061 Aluminum was selected as the mold material because of its superb thermal conductivity and manufacturability. The machined mold used in Sets 1-4 is shown in Figure 7.

Table 3. Mold dimensions

	Dimensions (*length x width x thickness*) (in)		
Sets	1-4	5	6
Base Plate	24 *x* 8.625 *x* 1	24 *x* 8.625 *x* 1	24 *x* 8.625 *x* 1
Short Frame Rails	6.625 *x* 1 *x* 1	6.625 *x* 1.5 *x* 1	6.625 *x* 2.5 *x* 1
Long Frame Rails	24 *x* 1 *x* 1	24 *x* 1.5 *x* 1	24 *x* 2.5 *x* 1
Caul Plate	22 *x* 6.620 *x* 1	22 *x* 6.620 *x* 1	22 *x* 6.620 *x* 1

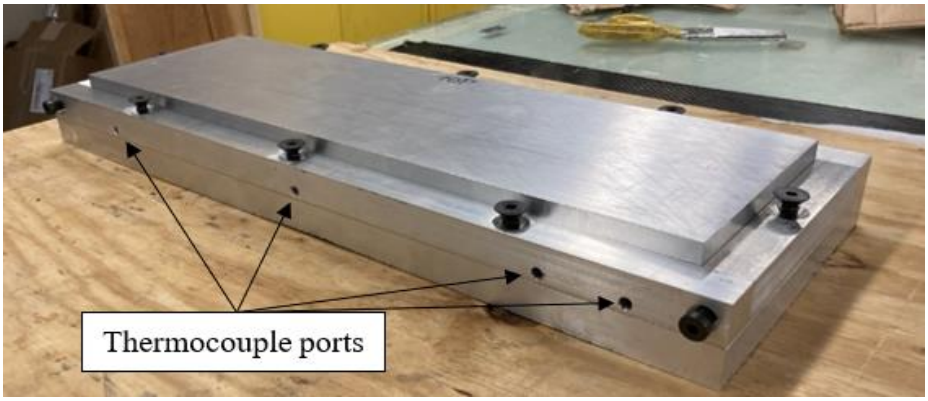

Figure 7. Aluminum 6061 matched tool mold

In the processing parameter study, four thermocouples were inserted into the composite between the seventh and eighth ply through machined ports to provide accurate temperature information throughout the process. The thermocouples used were fiberglass-insulated welded-tip Type K thermocouples with an operating range of 14ºF to 932°F. An AZ Instrument 4-channel logger was used to record temperatures measured by each thermocouple. The thermocouple locations for the processing parameter study were initially chosen according to their unique proximity to each frame rail as shown in Figure 8. It was hypothesized that the aluminum rails would provide additional thermal conductivity to the perimeter of the composite panel and thus the thermocouples were expected to provide a symmetric thermal gradient map of the entire composite panel during processing. It was later discovered that the temperature of specific points in the panel depended more on the proximity to the location of the heating elements and cooling channels and less on the proximity to the frame rails. As such, the thermocouple locations were moved to the center of the mold for the thickness study.

Two thermocouples were placed ¼ distance from the bottom and top of the panel and the remaining two were placed in the middle. This setup, illustrated in Figure 9, aimed to capture the thermal effect through the thickness of the panel as heat was conducted from the bottom and top platens. In both studies, each thermocouple was embedded in the composite after solidification, the remaining wire was trimmed externally at the port entrance and the area surrounding the thermocouple wire within the composite was not used for testing. In the 1 in panel, a total of 107 plies of Toray unidirectional material was used. Thermocouples 1-4 were placed at 23, 45, and 68 plies, respectively. In the 2 in panel, the maximum amount of plies the 2.5 in frame rails could accommodate was 192, with thermocouples 1-4 placed at 48, 96, and 144 plies respectively.

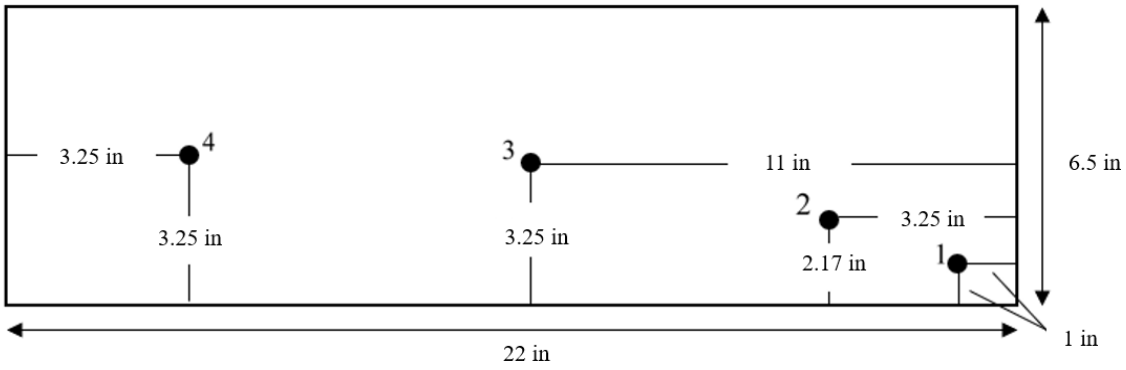

Figure 8. Sets 1-4 thermocouple locations (top view)

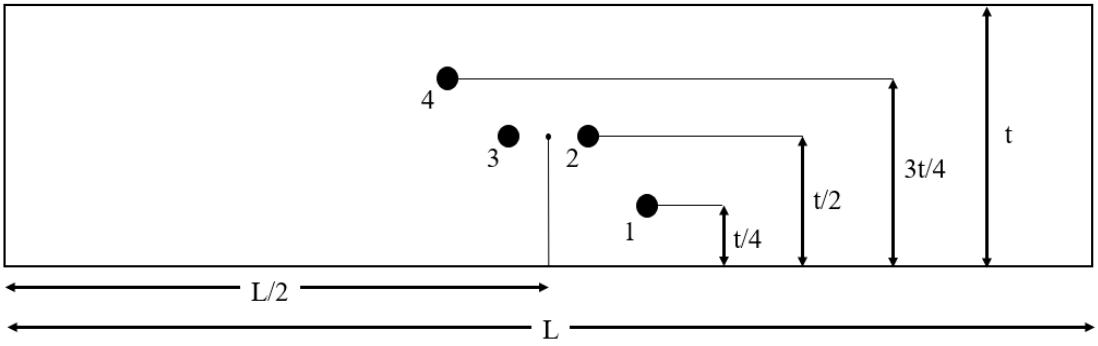

Figure 9. Sets 5-6 thermocouple locations (side view)

3.3. Test Procedures

3.3.1. Test Matrix

Using information received during a review of literature, a test matrix was generated to characterize the effects of processing parameters and thickness on PET/GF composites. Then a baseline recipe of low-end parameters suggested by literature was used that included a PPT of 450°F, 30 psi pressure, 1 min dwell, and a cooling rate of 12.5°F/min. Following the baseline, the PPT was analyzed at 470°F and 490°F to determine any significant changes in properties. The temperature at which the best properties was seen, denoted *A* in Table 4, was used in subsequent samples. Then, the pressure was adjusted to 60 psi and 90 psi and any changes in properties were noted. The best pressure, denoted *B*, was used in later samples. This method was repeated for dwell and cooling rate, denoted *C* and *D*, respectively. After manufacturing and

testing nine samples, an optimal processing recipe was determined and utilized in a further study investigating the effects of composite thickness on overall properties. Two thick-section panels were produced with target post-consolidation thicknesses of 1 and 2 in.

Table 4. Test matrix with parameter study (samples 1-9) and thickness study (samples 10-11)

Sample	Thickness (in)	Peak Processing Temp. (°F)	Pressure (psi)	Dwell (min)	Cooling Rate (°F/min)
1	0.125	450	30	1	12.5
2	0.125	470	30	1	12.5
3	0.125	490	30	1	12.5
4	0.125	*A*	60	1	12.5
5	0.125	*A*	90	1	12.5
6	0.125	*A*	*B*	15	12.5
7	0.125	*A*	*B*	30	12.5
8	0.125	*A*	*B*	*C*	5
9	0.125	*A*	*B*	*C*	20
10	1	*A*	*B*	*C*	*D*
11	2	*A*	*B*	*C*	*D*

3.3.2. Tensile Test

Tensile testing was conducted with each of the specimens listed in Table 4 according to ASTM D3039 [26]. Both 0° and 90° directions were tested using between 4 and 6 specimens per sample. The 0° tensile specimens were 9.85 in *x* 0.60 in *x* 0.125 in with 2.2 in *x* 0.60 in *x* 0.06 in thick fiberglass gripping tabs adhesively bonded to the composite specimen using epoxy thermoset resin. The 90° tensile specimens were 6.3 in x 1 in x 0.125 in. The standard calls for a length of 6.9 in, however, the total laminate width was limited by the Toray UD tape width of 6.5 in. 1 in *x* 1 in *x* 1.5 mm tabs will be adhesively bonded to the ends of the laminate for gripping purposes. The 0° and 90° specimen drawings are illustrated in Figure 11. The test apparatus used for 0° tensile testing was an MTS Criterion Model 45 fitted with a 78.7 kip (350 kN) load cell. The apparatus used for 90° tensile testing was Instron 5567 load frame and an MTS Criterion

Model 43 fitted with a 6.7 kip (30 kN) load cell. Each specimen was paired with an MTS Model 632.11B-20 extensometer with a gage length of 1 in to measure longitudinal displacement as displayed in Figure 10. A constant head displacement rate of 0.079 in/min (2 mm/min) was used for each test according to ASTM D3039. The tensile stress, σ, will be calculated using Eq. 1 where *P* is the load and *A* is the cross-sectional area of the test specimen. The maximum stress that the specimen endures before failure is its ultimate tensile strength. The tensile strain, ε, was calculated using Eq. 2 where δ represents the displacement of the extensometer and *L* is the extensometer gage length. Using the tensile stress and strain, the tensile modulus of elasticity, *E*, can be found using Eq. 3. This value represents the stiffness of the material in the elastic region of the stress-strain curve.

Figure 10. 0° tensile test with extensometer

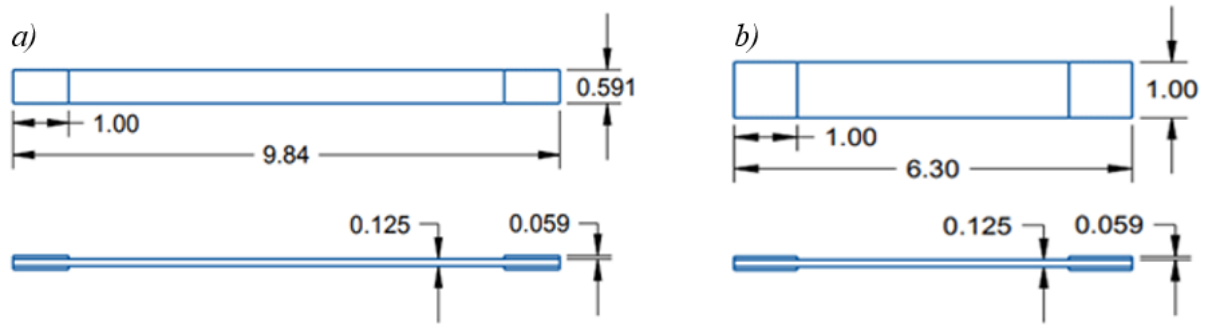

Figure 11. a) 0° tensile specimen geometry and b) 90° tensile specimen geometry

$$\sigma = \frac{P}{A} \quad \text{(Eq. 1)}$$

$$\varepsilon = \frac{\delta}{L} \quad \text{(Eq. 2)}$$

$$E = \frac{\sigma}{\varepsilon} \quad \text{(Eq. 3)}$$

3.3.3. Compression Test

Similar to tensile testing, a compression test was conducted in both 0° and 90° fiber orientations with 4 to 6 specimens tested per sample. The specimen size, shown in Figure 12, was 0.5 in *x* 0.5 in *x* 0.125 in, according to ASTM D695 [27]. Instron 5567 and MTS Criterion C30 load frames equipped with a 6.7 kip (30 kN) load frame were used to perform the tests. A compressive force was applied at a constant head displacement of 0.051 in/min (1.3 mm/min) until failure. Since the specimens are too small for extensometer implementation, the displacement will be measured according to the crosshead rate. Equations (Eqs.) 1-3 from the tensile tests will be used in a similar fashion to determine the compressive stress, strain, and elastic modulus. A stress-strain curve representing one typically seen for the tension and compression tests completed in this research is depicted in Figure A1.

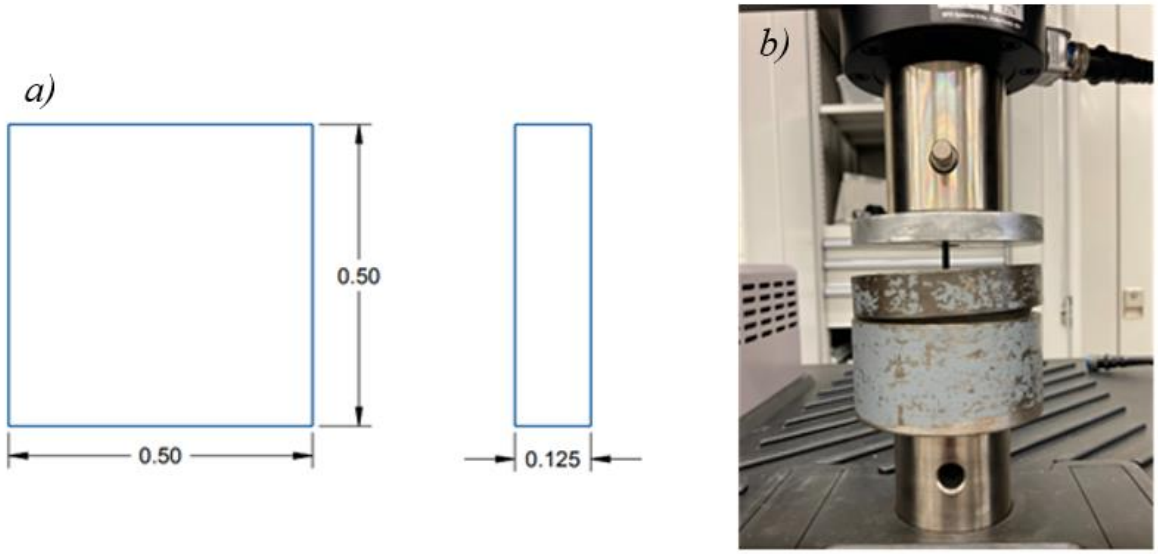

Figure 12. a) Compression specimen geometry and b) compression testing

3.3.4. Shear Test

The shear stress specimens were manufactured and tested according to the Interlaminar Shear Stress (ILSS) standards of ASTM D2344 as shown in Figure 13 [28]. The length and width are specified based on the laminate thickness. For a thickness of 0.125 in, the overall length is six times the thickness, or 0.75 in while the width is two times thickness, or 0.25 in. For shear testing, the span was the distance between the two supports which was specified as four times the thickness, or 0.5 in. The load was applied at a constant head displacement rate of 0.039 in/min (1 mm/min) until failure. The short beam shear strength, F, was calculated using Eq. 4 where P is maximum load, b is the specimen width, and h is the specimen thickness.

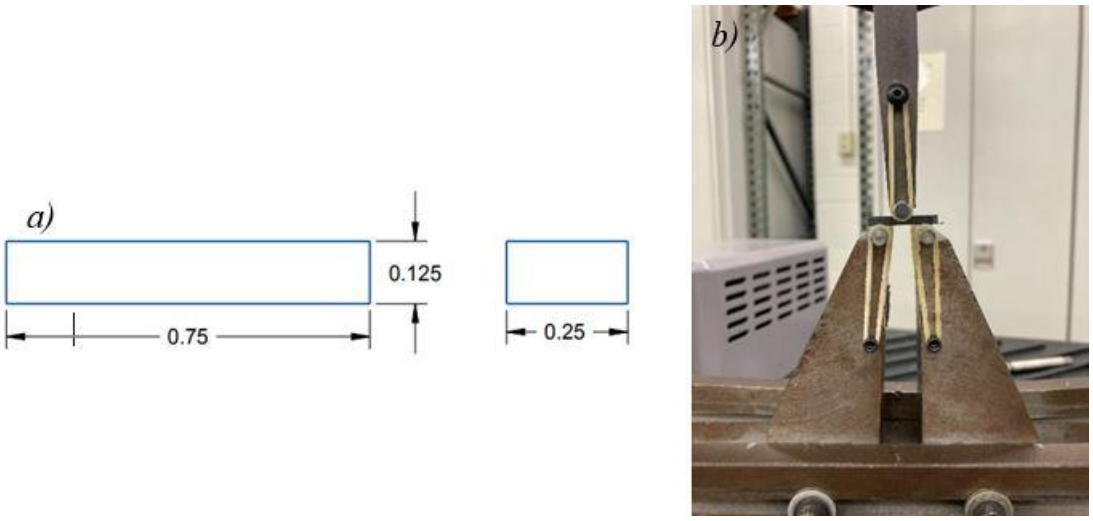

Figure 13. a) ILSS specimen geometry and b) ILSS testing

$$F = 0.75 \times \frac{P}{b \times h} \quad \text{(Eq. 4)}$$

3.3.5. Specimen Cutting

The tensile, compression, and shear test specimens were cut from the compression-molded panels using a Maxiem 1515 waterjet manufactured by OMAX (see Figure 14). CAD drawings, similar to those shown in Figures 11-13, were uploaded to the program and cut with a high-precision abrasive and water combination. Because different areas on the panels underwent different heating and cooling cycles, each of the various testing specimens were cut from the same locations on the panels for each run as seen in Figure 15. Because the waterjet leaves a tab on each of the cutouts for retainment, the compression specimens were wet sanded to eliminate the tab from testing surfaces.

Figure 14. a) Maxiem 1515 waterjet [29] and b) waterjet cutting 2 in sample

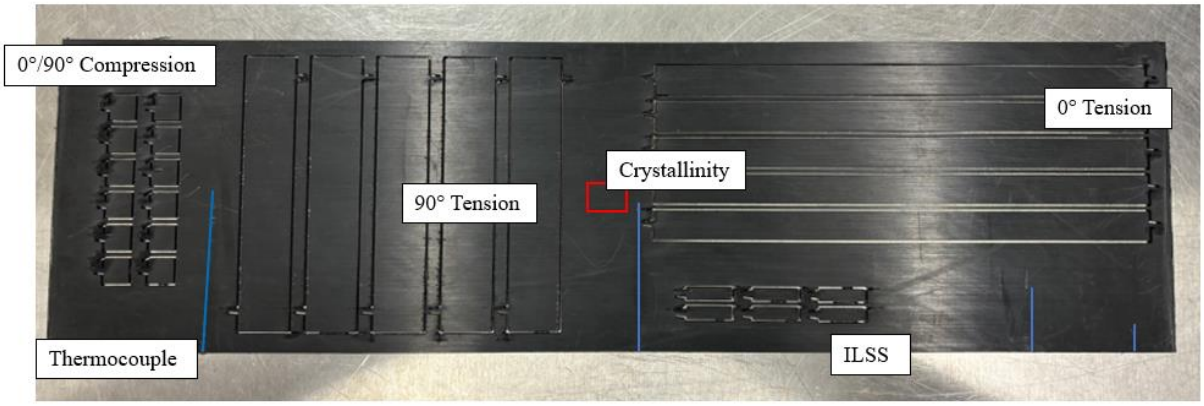

Figure 15. Diagram of all test specimen locations on molded panel

3.3.6. Specimen Dimensions in Thick-section Study

In the processing parameter study, the panel thickness of 0.125 in was defined in correspondence with ASTM standard specimen size recommendations. To create a level comparison to these results with regards to percent crystallinity, the thick-section study specimen geometries remained the same. First, the waterjet was used to cut out the specimen length and width from the panel. Then, a wet saw was used to slice the required thickness. In the 1 in panel, three 0.125 in sections were extracted from the top, middle, and bottom of each sample. Likewise, five 0.125 in sections were cut from the 2 in panel equidistant from each other. This process is illustrated in Figure 16.

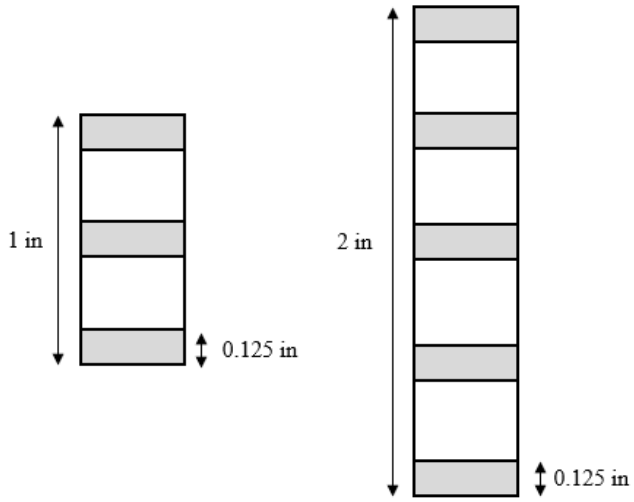

Figure 16. Thick-section specimen locations

3.3.7. Thermogravimetric Analysis

Before crystallinity testing was performed, the thermal degradation temperature of the Toray PET was determined to avoid damage to differential scanning calorimetry equipment. To accomplish this, thermogravimetric analysis, or TGA, was performed on a TGA Q500 testing apparatus, shown in Figure 17, according to ASTM D3850 [30].

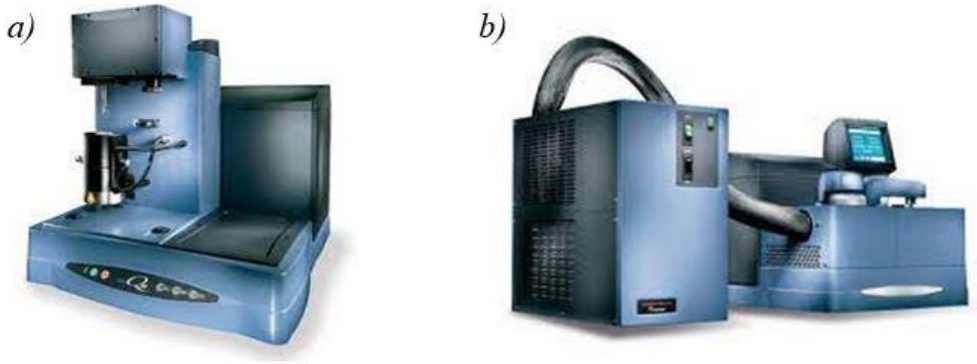

Figure 17. a) TGA Q500 [29], and b) DSC Q1000 [30]

3.3.8. Differential Scanning Calorimetry

The crystallinity study was performed using differential scanning calorimetry (DSC). A DSC Q1000 test apparatus shown in Figure 17b was used according to ASTM D3418 [33]. 10-

30mg shavings of PMC were collected from the approximate center of the panel, or Location 3 in Figure 8, using a side cutter and analyzed for percent crystallinity. Between 3 and 5 specimens were taken for each sample while heat-cool-heat cycle was used as the method of analysis. Beginning at ambient temperature, the furnace heated the sample to 716°F at a ramp rate of 20.8°F/min before being cooled to -76°F at a rate of -20.8°F/min using nitrogen then was finally heated back to 716°F at 20.8°F/min. To calculate the percent crystallinity of the composite, the area under the fusion curve was found using the linear integration feature of Universal Analysis software. The base of the integrated peak was formed using the slope of the heat flow line after melting had completed, as shown in Figure 18. This value was then divided by 0.4 to account for the mass of the fiberglass present in the composite that was not melted during the heating cycle. This operation assumed that each DSC specimen contained exactly 60% fiber weight fraction according to Toray specifications. Lastly, this value was divided by 140 J/g, or the theoretical mass-normalized enthalpy of 100% crystalline PET [34]. This formula is shown in Eq. 5.

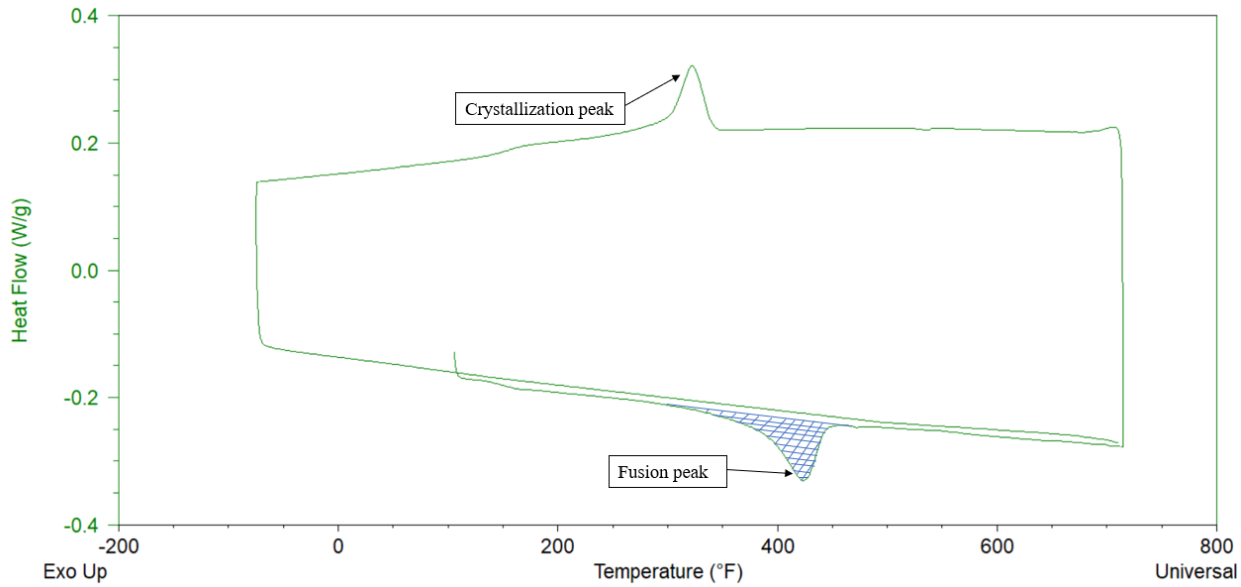

Figure 18. DSC graph with integrated fusion peak

Note: second fusion peak removed for clarity

$$\%\ crystallinity = \frac{(Mass\ norm.\ enthalpy/0.4)}{140} \times 100 \qquad \text{(Eq. 5)}$$

3.3.9. Statistical Analysis

One-factor analysis of variance (ANOVA) was performed on each of the combinations of processing parameters and thickness. One-factor ANOVA was chosen over multi-factor ANOVA due to the elimination procedure in which the data was collected. With four unique processing parameters and 3 options per parameter, there were 81 different combinations of parameters that would be required to run a true multi-factor ANOVA. Since this number of samples to manufacture and test was not feasible, a more efficient method was used. A limiting factor of one-factor ANOVA is that it only determined the effect of one parameter on the outcome and not the effect of changing two or more parameters. Because of this, the analysis did not provide a complete understanding of the molding parameters on crystallinity since variables such as temperature and pressure are interdependent. The null hypothesis was that the alteration of one parameter did not affect the percent crystallinity in the composite. A significant level of 5% was used to determine whether the null hypothesis could be rejected.

4. RESULTS

4.1. Set 1 – Temperature

The temperature profiles from Set 1 are shown in Figure 19. Beginning from ambient temperature, the PET took between 41 and 46 mins to reach the target temperatures of 450°F, 470°F and 490°F and the average maximum temperatures across all thermocouples before the cooling stage initiated was 447.3°F, 466.8°F, and 485.9°F, respectively. The initial hypothesis discussed in Section 3.2.2 that predicted the thermal conductivity of the aluminum frame would have the greatest effect on the composite temperature was incorrect. Rather, the location of the heating element and cooling channels within the press platens had the most impact on the temperature. Figure 20 shows this effect, as thermocouples 1, 2, and 4 follow roughly the same temperature profiles through heating and cooling while thermocouple 3 reaches the target temperature first before cooling at a much faster rate than the other thermocouples. Thermocouple 3 was located in the center of the mold, which laid directly beneath the platen heating element. The target cooling rate for this set was 12.5°F/min, with the average cooling rate across the panels in the 450°F, 470°F, and 490°F runs were 12.2°F, 12.5°F, and 12.4°F, respectively.

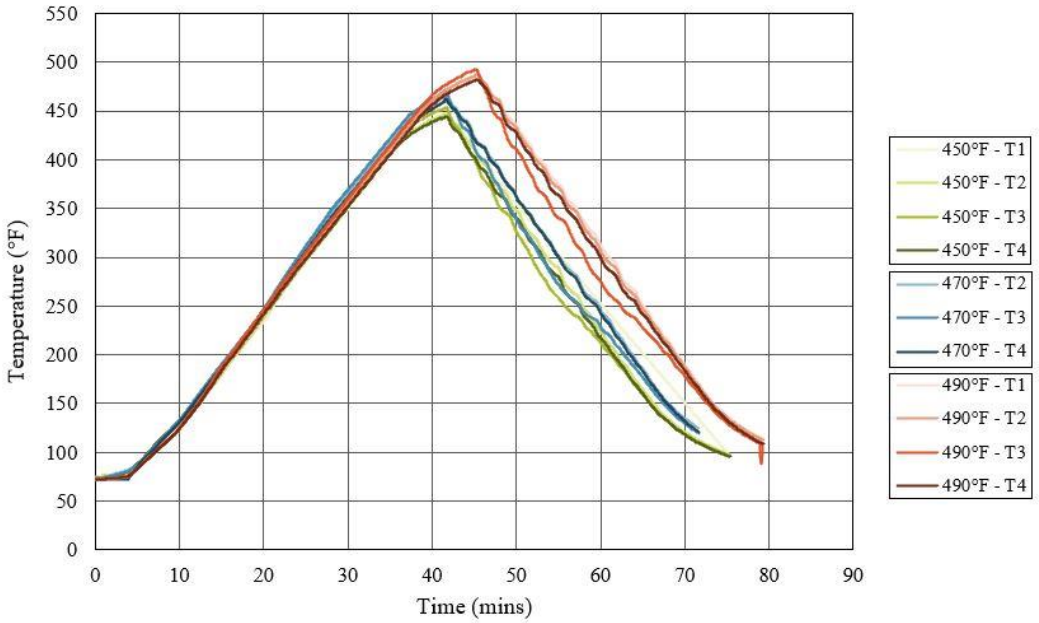

Figure 19. Set 1 temperature profiles

Note: T1 not shown due to malfunction during processing

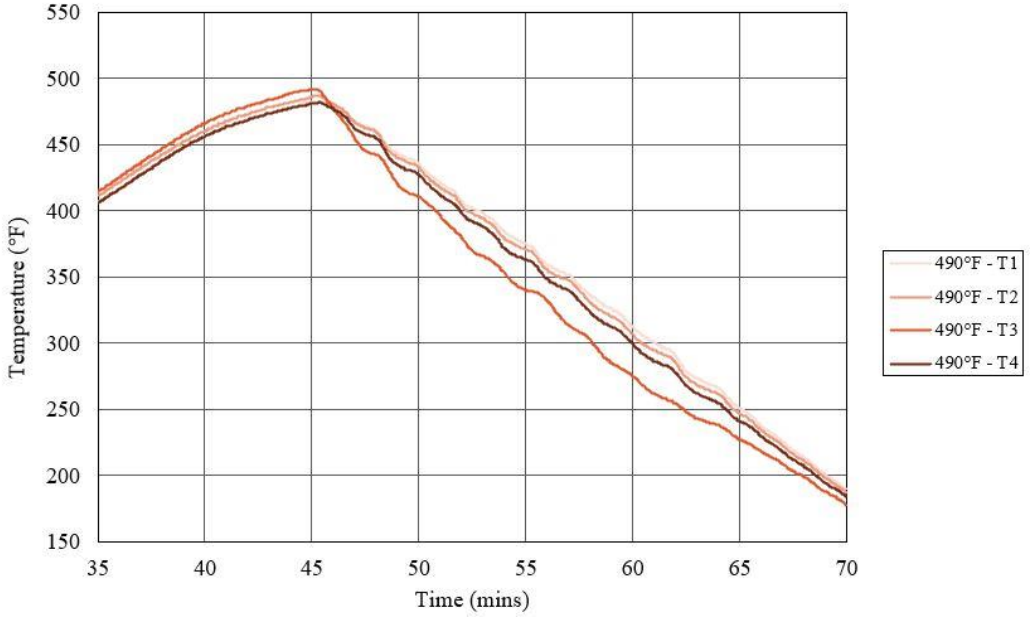

Figure 20. Close up showing 490°F cooling rate

During processing, the composite material experienced significant amounts of flashing as seen in Figure 21. Although the portion of the panels used for testing appeared to be of excellent quality, an underlying phenomenon occurred that proved to alter the structure and subsequent

mechanical properties of the overall material. As the PET is heated past its T_m, the viscosity decreases and allows it to flow through gaps between the mold components. Since the fiber only runs in one direction in a unidirectional composite, the flowing polymer pulls the fiber along with it as there is no reinforcing fiber in the longitudinal direction to contain it as illustrated in Figure 22. This effect is further compounded by the uneven pressure on the caul plate caused by the thermocouples inserted on one side of the mold. Figure 22 shows the post-processed mold with excessive PET and fiber flashing. This “fiber wash” effect degrades material properties, especially in the 0° direction and causes difficulty in getting true failure during testing. Many of these specimens failed as a result of delamination or tab adhesive rupture. For this reason, only elastic modulus was used in 0° tensile results.

Figure 21. Post-processed mold showing polymer and fiber flashing

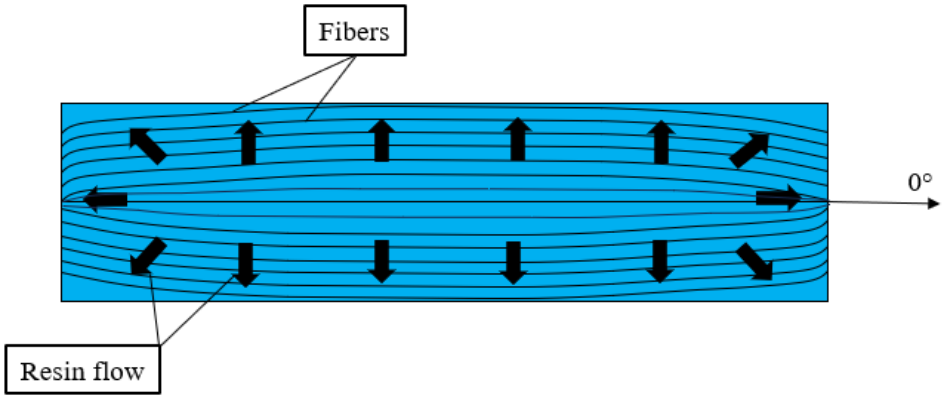

Figure 22. Diagram showing fiber wash in unidirectional PMC

The crystallinity of the 450°F, 470°F, and 490°F samples were 18.1%, 16.2%, and 18.6%, respectively, and the ANOVA proved each result to be non-significant at 95% confidence as depicted in Figure 23. The mechanical properties for Set 1 are shown in Figure 24 and Table 5. The abbreviations used to represent mechanical properties on all radar plots and tables are displayed in Table 6. Both the compression strength and modulus in the 0° direction, the compression modulus in the 90° direction, and the ILSS results proved to be significant. The 490°F specimens were the lowest in all categories except tensile modulus, which was insignificant. Although prior research has shown that increasing temperature may increase crystallinity and mechanical properties, this was untrue in this study. After compression molding at 470°F and 490°F PPT, it was clear that the higher temperatures had an adverse effect on the quality of the samples as there were several long thermal cracks along the length of the panel that were unseen in the 450° panel. It is likely that the thermal expansion and contraction of the aluminum frame amplified the stress on the panel at temperatures over the melting point of the polymer. For this reason, 450°F was chosen as the PPT for subsequent runs.

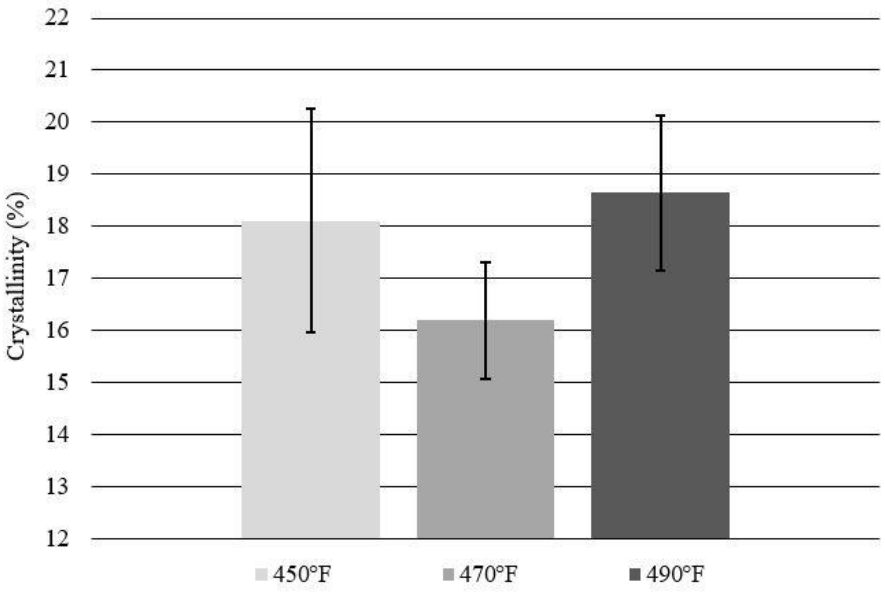

Figure 23. No significance seen in Set 1 crystallinity

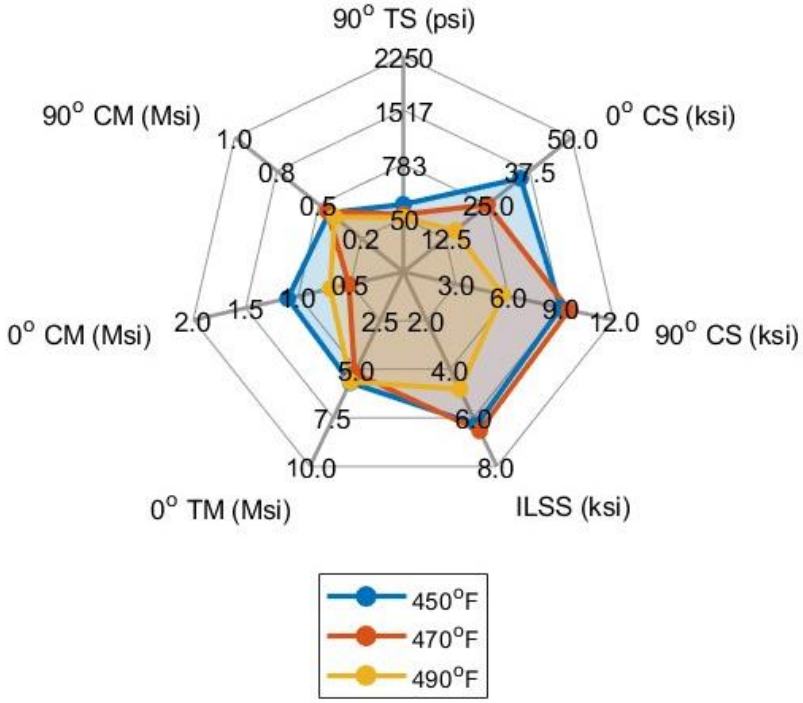

Figure 24. 450°F showing slightly greater 0° CS and CM [35]

Table 5. Tabulated Set 1 mechanical properties

Property	450°F, 30 psi, 1 min, 12.5°F/min		470°F, 30 psi, 1 min, 12.5°F/min		490°F, 30 psi, 1 min, 12.5°F/min	
	M	*SD*	*M*	*SD*	*M*	*SD*
90° TS (psi)	235.8	20.42	100.2	64.60	58.62	12.10
0° CS (ksi)	34.83	5.197	24.97	4.365	15.44	2.588
90° CS (ksi)	8.990	2.334	9.472	1.795	5.661	0.382
ILSS (ksi)	6.287	0.235	6.531	0.151	4.823	0.712
0° TM (Msi)	5.688	0.557	5.210	0.328	5.658	0.164
0° CM (Msi)	1.907	0.014	0.518	0.262	0.696	0.164
90° CM (Msi)	0.440	0.066	0.450	0.177	0.408	0.030

Table 6. Mechanical property abbreviations

TS	Tensile Strength
TM	Tensile Modulus
CS	Compression Strength
CM	Compression Modulus
ILSS	Interlaminar Shear Strength

4.2. Set 2 – Pressure

Set 2 analyzed the effect of altering pressure during the molding process. The baseline of 30 psi was increased to 60 psi and 90 psi. The temperature profiles appear very similar other than the higher pressures delivered a faster heating rate (see Figure 25). The crystallinity showed a slightly inverse relationship with pressure with the 60 and 90 psi samples scanning at 17.1% and 15.7%, respectively. However, these results were statistically insignificant as seen in Figure 26. The 0° compression modulus in the 30 psi sample was significantly greater than the 60 psi sample but both were insignificant compared to the 90 psi sample. The 30 psi sample also had significantly higher strength in the 0° direction than the 60 and 90 psi samples. With all other mechanical properties results being insignificant, 30 psi was chosen as the ideal pressure for this material.

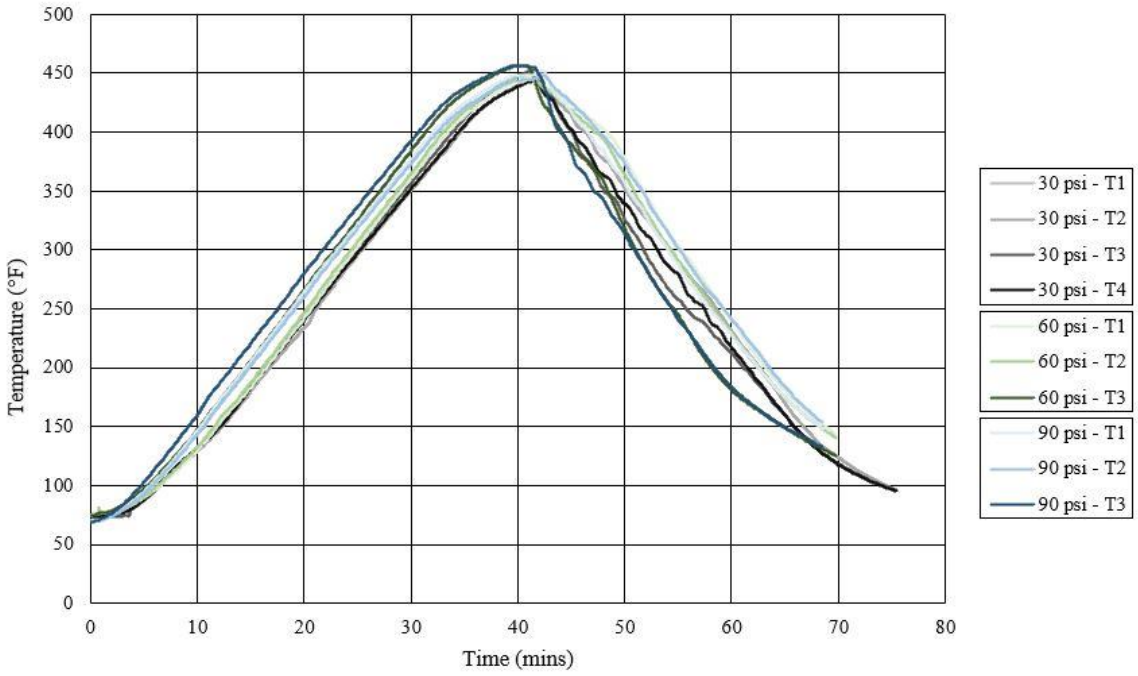

Figure 25. Slight temperature variations seen in 30, 60, and 90 psi samples

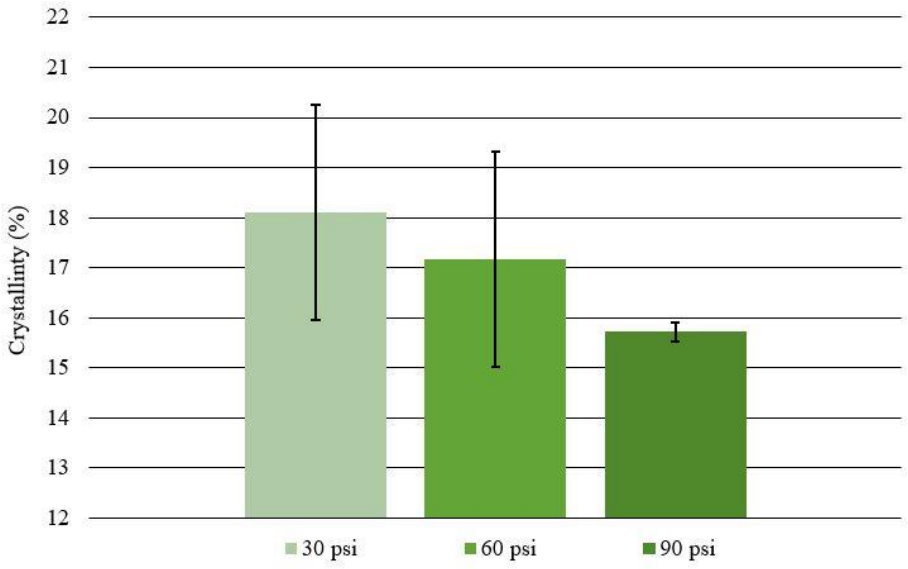

Figure 26. No significance differences in crystallinity from pressure change

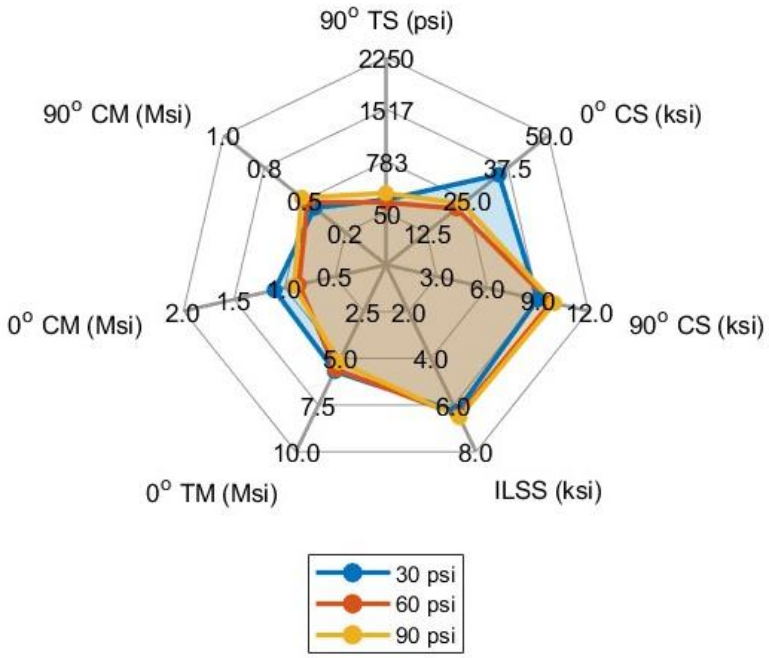

Figure 27. Increase in 0° CS in 30 psi sample

Table 7. Tabulated Set 2 mechanical properties

Property	450°F, 30 psi, 1 min, 12.5°F/min		450°F, 60 psi, 1 min, 12.5°F/min		450°F, 90 psi, 1 min, 12.5°F/min	
	M	*SD*	*M*	*SD*	*M*	*SD*
90° TS (psi)	235.8	20.42	199.5	82.52	330.5	91.82
0° CS (ksi)	34.83	5.197	21.73	1.659	23.61	3.756
90° CS (ksi)	8.990	2.334	9.778	0.711	9.968	1.230
ILSS (ksi)	6.287	0.235	6.437	0.338	6.515	0.484
0° TM (Msi)	5.688	0.557	5.592	0.496	5.208	0.269
0° CM (Msi)	1.907	0.014	0.860	0.133	0.908	0.139
90° CM (Msi)	0.440	0.066	0.484	0.031	0.520	0.038

4.3. Set 3 – Dwell

In Set 3, the dwell, or holding time at the PPT was altered in increments of 15 min. The second run was heated to approximately 450°F then held for 15 min before cooling was initiated. Similarly, the third run was heated to 450°F and held for 30 min. On the temperature profile shown in Figure 28, the 30 min panel appears to heat much quicker than the 15 min panel. This

is due to the oven being in a preheated state when the mold was inserted into the press. The average maximum temperature sustained during dwell was 451.4°F and 451.1°F, respectively. The average cooling rate across the panel was 12.5°F/min in the 15 min dwell and 12.3°F/min in the 30 min dwell.

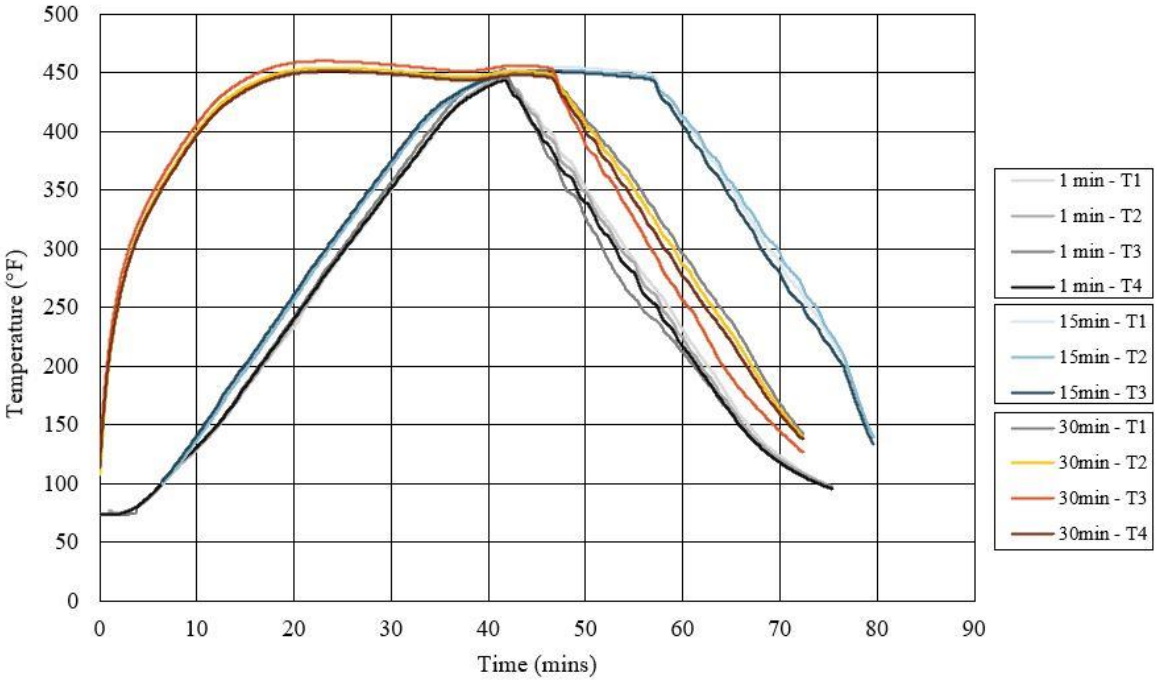

Figure 28. Dwell lengths shown in Set 3 temperature profiles

Increasing the dwell time proved to decrease the polymer crystallinity as the baseline sample of a 1 min dwell was 18.1% crystalline, which was significantly greater than 15.7% and 13.8% in the 30 and 15 min dwell, respectively (see Figure 29). As displayed in Figure 30 and Table 8, the 90° tensile strength was the most significant mechanical property, with the 15 min sample reaching over 2000 ksi, roughly 10 times greater than the 1 and 30 min samples. Similarly, the compression strength in the 90° direction was significantly greater than the alternatives at 11.6 ksi. In the 0° direction, the compression strength was greater in the 15 and 30 min dwell than the baseline and while not significant between each other, the modulus of all three dwell periods was higher than all other treatment combinations. Lastly, the 15 min sample

performed the highest in ILSS at 6.8 ksi, which was 8.1% and 11.0% greater than the 1 and 30 min dwell, respectively. Despite the 15 min dwell sample showing increased mechanical properties, the 1 min dwell was utilized in the remainder of the study due to its higher level of crystallinity.

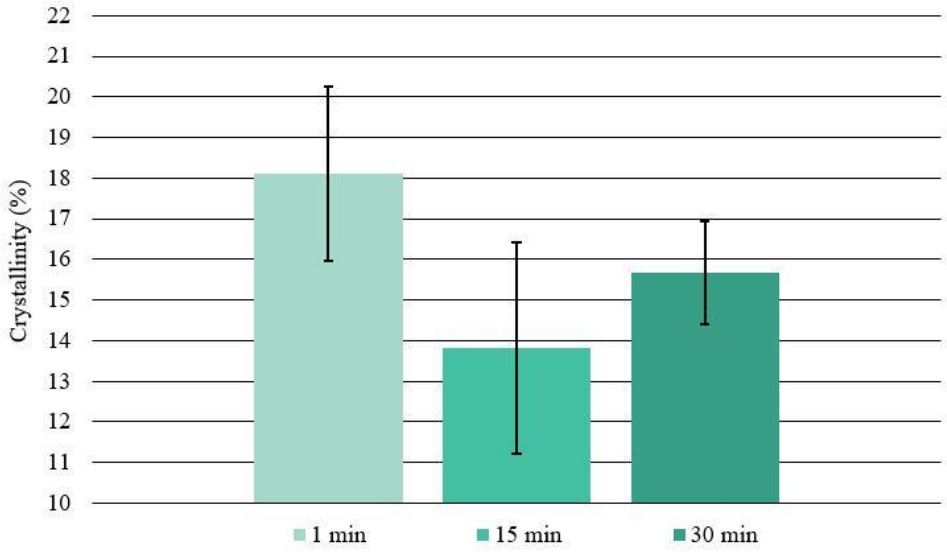

Figure 29. No significance seen in crystallinity from dwell increase

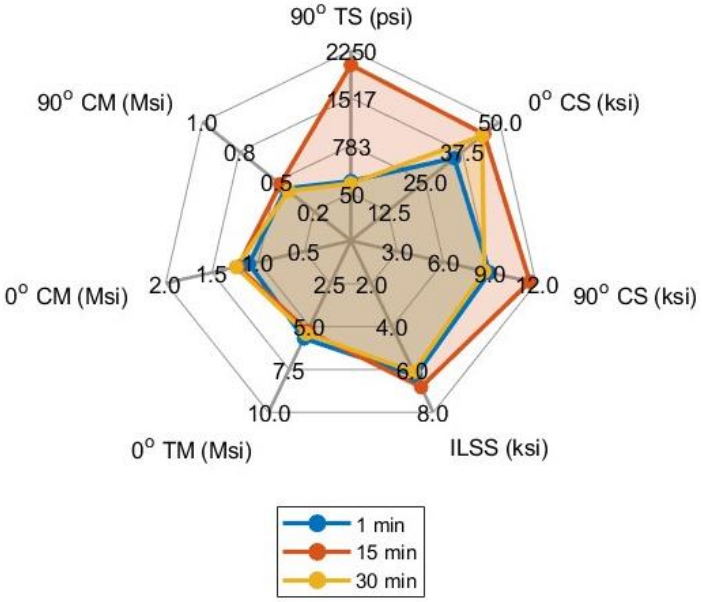

Figure 30. 15 min dwell significantly increased mechanical properties

Table 8. Tabulated Set 3 mechanical properties

Property	450°F, 30 psi, 1 min, 12.5°F/min		450°F, 30 psi, 15 min, 12.5°F/min		450°F, 30 psi, 30 min, 12.5°F/min	
	M	*SD*	*M*	*SD*	*M*	*SD*
90° TS (psi)	235.8	20.42	2026	315.1	197.6	62.12
0° CS (ksi)	34.83	5.197	44.94	13.67	44.21	8.025
90° CS (ksi)	8.990	2.334	11.56	1.539	8.641	2.025
ILSS (ksi)	6.287	0.235	6.821	0.121	6.107	0.123
0° TM (Msi)	5.688	0.557	5.255	0.624	5.407	0.399
0° CM (Msi)	1.907	0.014	1.221	0.258	1.246	0.126
90° CM (Msi)	0.440	0.066	0.477	0.064	0.419	0.032

4.4. Set 4 – Cooling Rate

Figure 31 shows the temperature profiles of Set 4 in which the cooling rates were studied. The two other rates targeted were 5°F/min and 20°F/min compared to the baseline of 12.5°F/min. The composites were first heated to 451.0°F and 449.8°F, then cooled at rates of 6.0°F/min and 18.8°F/min, respectively. In the slow cooling profile, at the beginning of the cooling stage, there are sections of time in which the cooling rate appears to be altered drastically. This is due to the required manual adjustment of the water input to the press. In its automatic setting, the press utilizes both air and water cooling to reach a desired temperature after a specified amount of time, however, the volume of water allowed into the system by the valve had an effect as well. If the temperature reading of the platens showed a considerable difference compared to the setpoint, the position of the valve was adjusted to increase or decrease the cooling rate accordingly. Although a smooth temperature curve is not shown in the profile, the average cooling rate remained close to the targeted 5°F/min so the panel was deemed acceptable to test.

While there was no significance between the 12.5°F/min and 20°F/min cooling rates, the 5°F/min rate increased to 28.5% which was nearly 1.5 times greater than the alternatives. This treatment combination has the most significant effect on crystallinity compared to all other treatments studied. After the 15 min dwell sample, the 20°F/min and 5°F/min samples had the highest 90° tensile strength at 1454.4 psi and 681.2 psi, respectively, which were both significant at 95% confidence. Conversely, the baseline cooling rate had a higher 0° tensile modulus than the alternatives. In compression, all results were insignificant except for 0° modulus in which the baseline was slightly greater than the 5°F/min and 20°F/min (see Figures A2-A7). During the analysis of the DSC results, a mistake was made during the initial calculations, and it appeared that there was no significance between the crystallinity of the three cooling rates. However, once the mistake was discovered, the 1 in and 2 in panels were already processed. For this reason, the 12.5°F/min cooling rate was used in the thickness study.

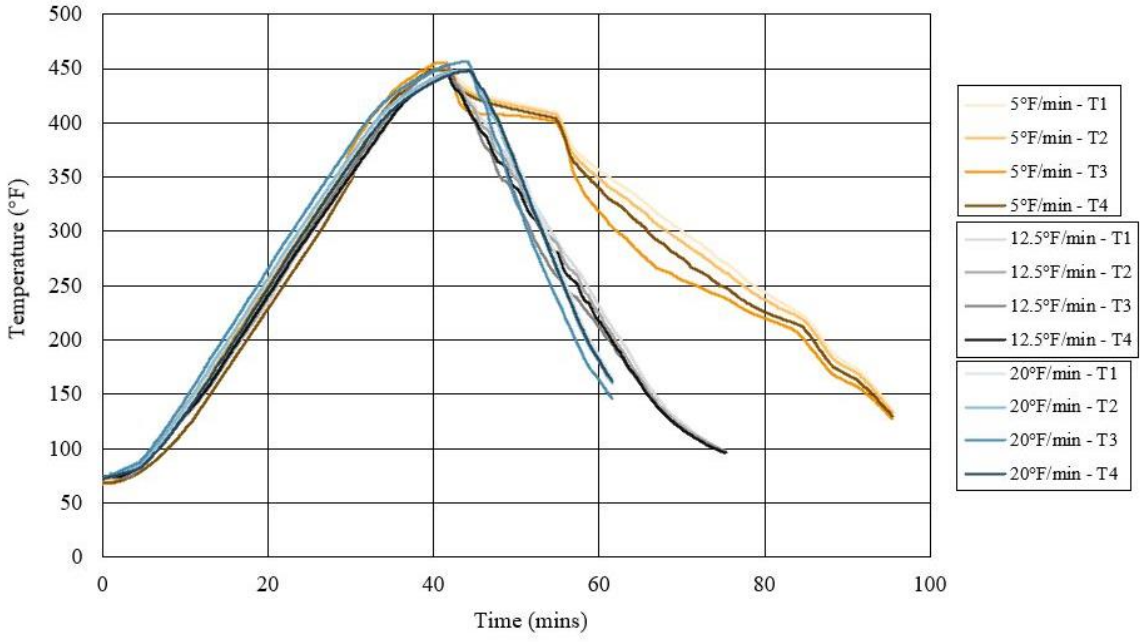

Figure 31. Temperature profiles of altered cooling rates

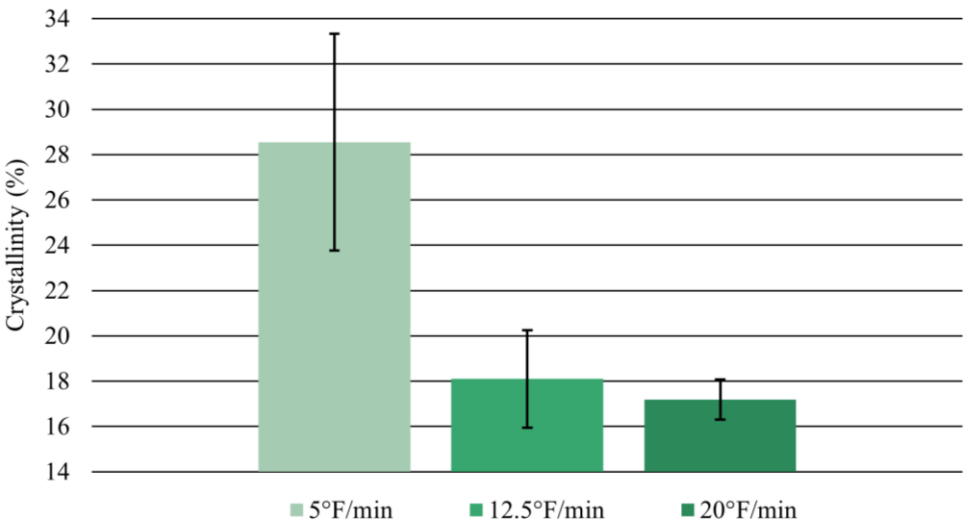

Figure 32. 5°F/min cooling rate increased crystallinity by over 10%

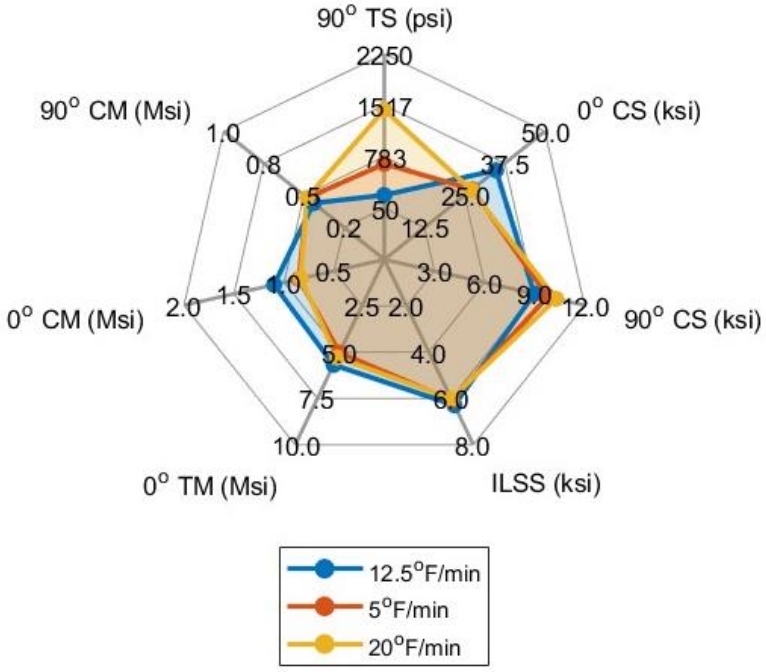

Figure 33. Mixed mechanical property results between cooling rates

Table 9. Tabulated Set 4 mechanical properties

Property	450°F, 30 psi, 1 min, 12.5°F/min		450°F, 30 psi, 1 min, 5°F/min		450°F, 30 psi, 1 min, 20°F/min	
	M	*SD*	*M*	*SD*	*M*	*SD*
90° TS (psi)	235.8	20.42	681.2	328.1	1454	274.1
0° CS (ksi)	34.83	5.197	27.42	2.438	27.14	1.979
90° CS (ksi)	8.990	2.334	9.794	1.127	10.34	0.658
ILSS (ksi)	6.287	0.235	6.080	0.147	6.010	0.277
0° TM (Msi)	5.688	0.557	5.034	0.348	5.288	0.252
0° CM (Msi)	1.907	0.014	0.852	0.051	0.835	0.098
90° CM (Msi)	0.440	0.066	0.480	0.057	0.481	0.049

4.5. Set 5 – 1 in Thickness

The 1 in panel consolidated well inside the larger mold and there were no qualitative signs that suggested a large void content and no stress cracks were present through the cross-section, as seen in Figure 34. The temperature profile shows slight variation between each thermocouple, meaning the composite heated relatively uniformly through the thickness and a crystallinity gradient was not likely to form (see Figure 35).

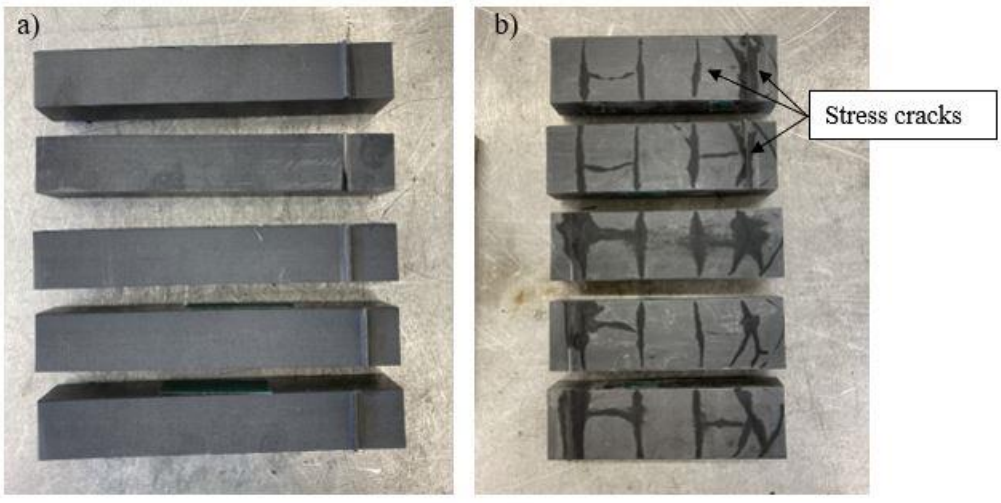

Figure 34. a) 1 inch and b) 2 inch 90° tensile samples prior to layer slicing

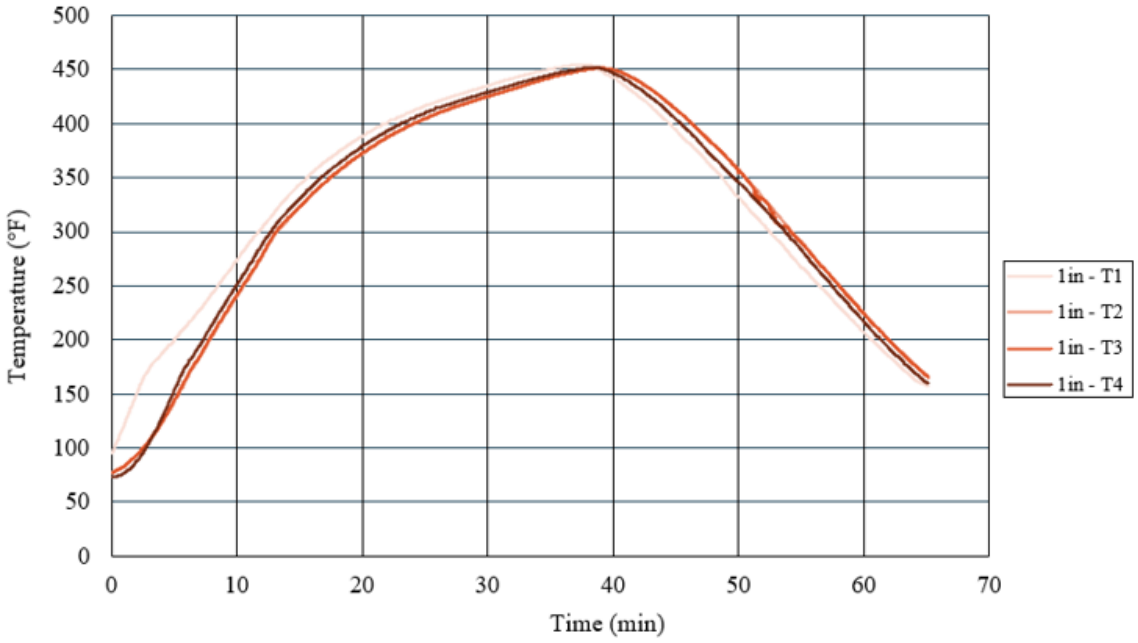

Figure 35. Temperature profile collected during 1 in sample processing

Expectedly, insignificant differences in percent crystallinity were seen throughout the thickness of the 1 in sample (see Figure 36). In interlaminar shear, the middle section of the panel had the greatest strength, and the top section was the weakest but both samples were not significantly different than the bottom section. Compression modulus was the only other property with significance in which the bottom section was more ductile in the 0° direction than the top and the middle sections. In the 90° directions, the top section was the stiffest compared to the middle and bottom sections. Overall, there was no clear indication of any symmetry regarding mechanical properties through the cross-section of the 1 in panel as shown in Figure 37 and Table 10.

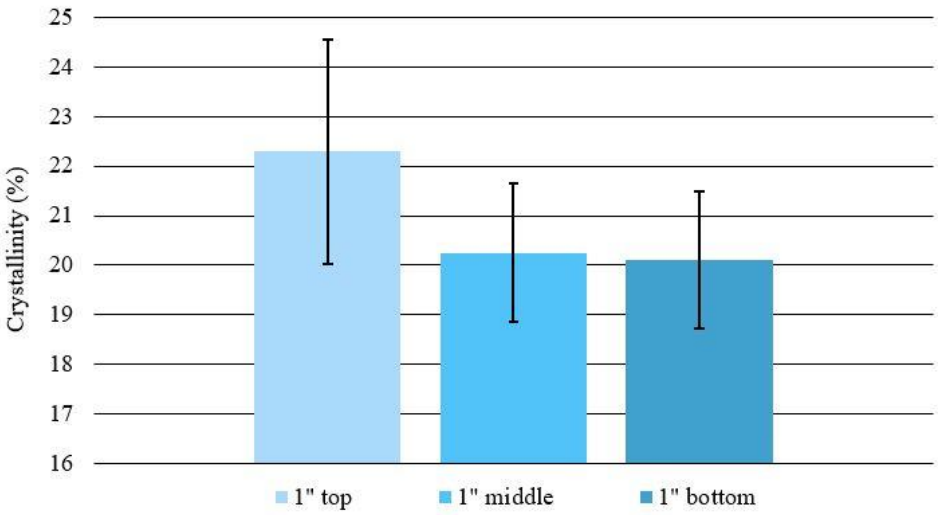

Figure 36. No significance in crystallinity seen through 1 in cross-section

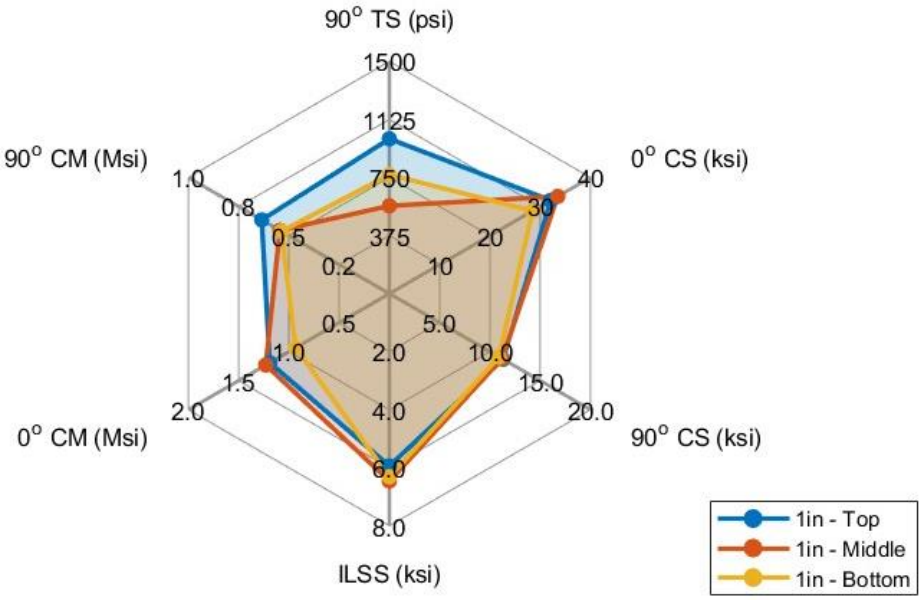

Figure 37. Slight gradient seen in 90° TS between layers

Table 10. Tabulated Set 5 mechanical properties

Property	1 in - Top		1 in - Middle		1 in - Bottom	
	M	*SD*	*M*	*SD*	*M*	*SD*
90° TS (psi)	999.5	458.9	567.4	254.3	768.3	403.2
0° CS (ksi)	32.09	2.760	33.53	6.064	28.45	5.801
90° CS (ksi)	11.35	0.936	11.22	1.231	10.91	1.072
ILSS (ksi)	5.941	0.138	6.461	0.265	6.310	0.464
0° CM (Msi)	1.192	0.138	1.237	0.099	0.933	0.258
90° CM (Msi)	0.635	0.028	0.545	0.027	0.537	0.042

4.6. Set 6 – 2 in Thickness

The 2 in panel required over 160 mins to complete the heating and cooling cycle, as shown in Figure 38. Although a 65°F temperature difference between T3 and T4 was present during the cooling stage causing an approximate 8 min lag between the inner and outer sections of the panel, a similar temperature difference occurred on the heating stage. Essentially, all sections through the thickness of the sample experienced the same thermal profile but at different times throughout the process. Therefore, it was expected that there would be no significant differences in crystallinity or mechanical properties. Qualitatively, an interesting phenomenon appeared after cutting the 90° tensile specimens. As illustrated in Figure 34, water spots highlighted several cracks in the sample and due to their symmetry between specimens it was evident that significant thermal stress occurred throughout the entirety of the panel. It is possible that the taller aluminum frame rails attributed to more thermal stress on the 2 in panel during cooling. Attempts were made to slice the 90° tensile samples into testable specimens, but the excessive number of cracks prevented this operation, and it was determined to eliminate this test from the matrix in Set 6.

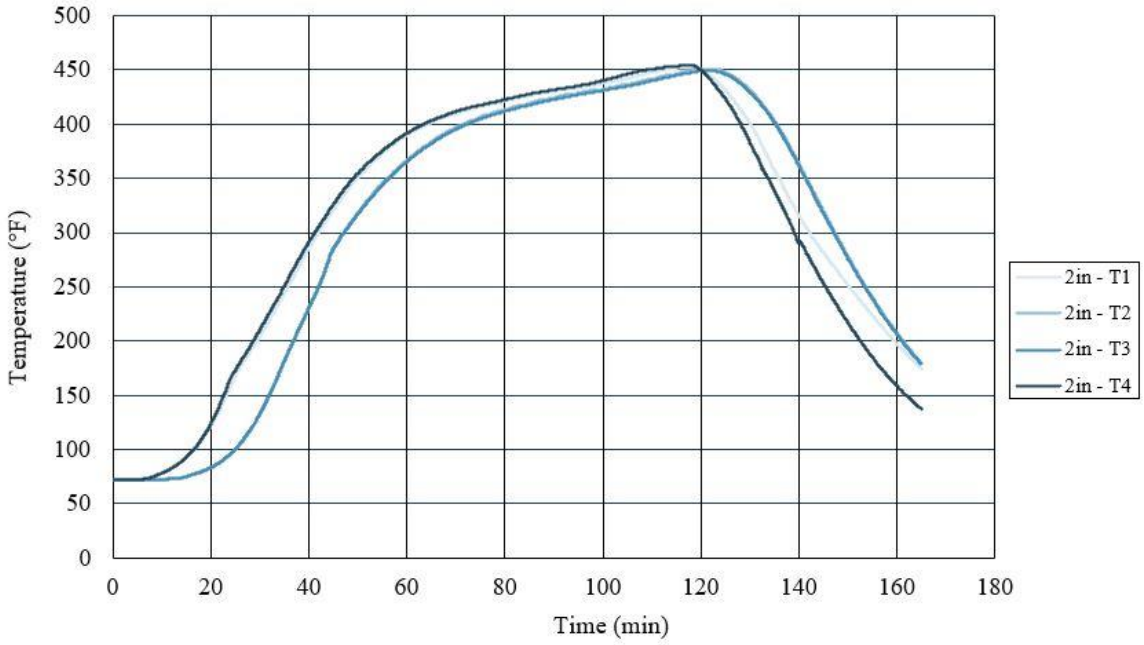

Figure 38. Roughly 8 min lag seen between T1/T4 and T2/T3 thermocouples

As depicted in Figure 39, the DSC results showed that the mean crystallinity fell between 22-23% in each of the five samples through the thickness of the panel. The top and top-middle sections were the strongest and stiffest in compression and significant strength differences were only seen in 0° where the top-middle was stronger than the middle and bottom-middle. Regarding modulus, the top, top-middle, and bottom sections were stiffer than the middle and bottom-middle sections in the 0° direction and the top section had a significantly greater modulus compared to the rest of the samples (see Figures A13-A15).

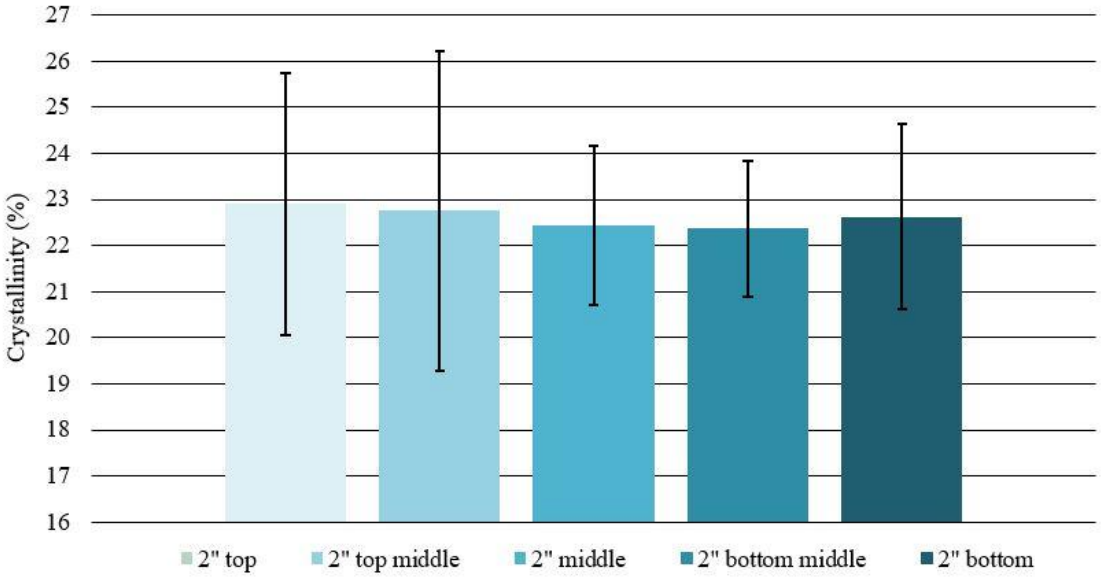

Figure 39. Mean crystallinity remained between 22-23% throughout 2 in sample

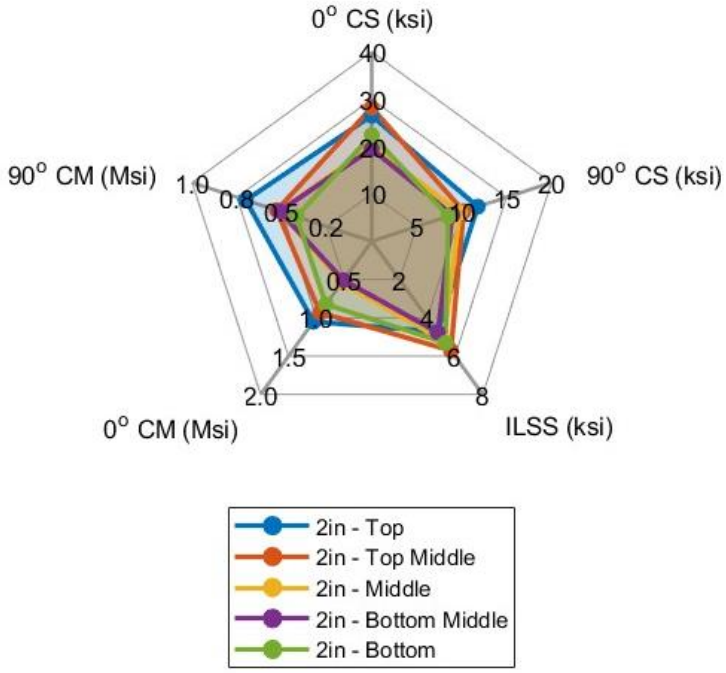

Figure 40. Scattered mechanical property data collected in 2 in study

Table 11. Tabulated Set 6 mechanical properties

Property	2 in - Top		2 in – Top Middle		2 in - Middle		2 in – Bottom Middle		2 in - Bottom	
	M	*SD*	*M*	*SD*	*M*	*SD*	*M*	*SD*	*M*	*SD*
0° CS (ksi)	26.48	4.600	28.20	7.273	20.09	4.970	19.53	4.648	22.41	1.971
90° CS (ksi)	11.84	6.594	10.23	0.988	9.806	1.530	8.980	1.660	8.515	0.722
ILSS (ksi)	4.734	0.695	5.706	0.751	5.204	0.289	4.765	0.575	5.314	0.296
0° CM (Msi)	1.051	0.105	0.932	0.219	0.543	0.226	0.509	0.067	0.825	0.064
90° CM (Msi)	0.701	0.231	0.529	0.072	0.513	0.041	0.514	0.046	0.419	0.036

5. DISCUSSION

One objective of this study was to determine the effect of compression molding processing parameters on composite properties. It was hypothesized that altering the PPT, pressure, dwell period, and cooling rate independently would produce changes in crystallinity and subsequently effect the strength and stiffness of a GF-reinforced PET composite. From the DSC data, the only parameter that had a significant impact on crystallinity was the cooling rate. The slowest cooling rate, 5°F/min, produced a crystallinity level nearly 50% greater than the next best treatment combination. This result corroborated similar studies that show that increasing the duration of the cooling process allows more time for the polymer microstructure to develop into crystals [20], [36]. While percent crystallinity may have increased as a result of slowing the cooling rate, a higher crystallinity did not correlate to improved mechanical properties as hypothesized. For example, the 90° tensile strength was greater in the 5°F/min sample than the majority of other treatment combinations in the study but this effect was negated by the quickest cooling rate, 20°F/min, producing a strength two times higher than 5°F/min. Additionally, the baseline cooling rate of 12.5°F/min demonstrated the highest tensile and compression modulus in the 0° direction.

The hypothesis of a positive correlation between percent crystallinity and mechanical properties was also disproved by the results of the dwell study. Despite having the lowest crystallinity level, the 15 min dwell sample recorded the greatest values in both 0° and 90° compression, ILSS, and most impressively, a 90° tensile strength that was over ten times greater than the 1 min and 30 min dwell. Conversely, increasing the PPT to 490°F in Set 1 produced the second-highest crystallinity percentage but remained in bottom third in 6 out of 7 mechanical property tests, including 90° compression and ILSS in which it had drastically lower results

compared to all other treatments. This was a particularly interesting result as the manufacturer's lowest recommended processing temperature was 490°F. Since each of these properties are largely matrix-dominant, this result suggests that a separate polymeric property such as interfacial adhesion to the glass fibers or stress cracking within the matrix had a larger effect on its performance than percent crystallinity. It was clear in the higher PPT runs of Set 1 that there were many more cracks spanning the entire panel than any other parameter variation which indicated there were likely smaller sub-cracks present in the test specimens as well. Additionally, the fiber washing effect that took place in the unidirectional PMC likely contributed an unmeasurable amount on the mechanical properties, specifically in the 0° direction. This phenomenon was demonstrated in Set 2 in which the 60 and 90 psi samples performed lower than the 30 psi samples. The increased pressure caused more resin flow and thus magnified the amount of fiber misalignment.

It was evident that matrix-dominant properties were not directly proportional to dwell since the properties appeared to reach a peak at 15 mins then returned to similar values at 30 mins compared to 1 min. In a similar study investigating the effect of PPT and holding time, Fugihara et al. discovered that by increasing the hold time from 20 to 60 mins significantly decreased the bending strength of carbon/PEEK composites [19]. This was attributed to increased amounts of sub-cracks throughout the matrix which likely stemmed from the degradation of the PEEK. The TGA performed at the start of this research shows a degradation temperature of approximately 820°F for this Toray PET which immensely exceeds the PPT used during any treatment, so it is more likely that increasing dwell beyond 15 mins attributed to some degree of PET degradation (see Figure A2).

It was anticipated that as the thickness of the compression molded panel increased, a larger crystallinity gradient would manifest through the layers of the panel. This hypothesis was rejected as there was no clear evidence in the crystallinity or mechanical property results that pointed to this correlation. When reviewing the thermocouple data, other than the offset in time, the inner sections of the panel experienced nearly the same heating and cooling cycle as the outer sections, so this result was a logical conclusion. Perhaps there were differences in void content or level of sub-cracks present through the cross-section, but this was not suggested by the scattered mechanical property data collected. The general trend in the thick-section study showed that the mechanical properties, especially in the 0° direction, were greater in the outer sections compared to the inner sections, with exception to ILSS in the 1 in panel. While it was difficult to see a clear correlation from the inconsistent findings, it is possible that the top and bottom sections of the sample experienced more fiber wash due to the fact that those layers reached the T_m of the PET quicker than the middle layers. Additionally, once the polymer in the middle reached the PPT the upper layers would shortly begin the cooling cycle in which the PET would consolidate and prevent more flashing and fiber wash out of top of the mold. This hypothesis was only speculative, however, as no optical images were taken or fiber misalignment measured during this study but this effect could perhaps could be investigated in later research.

6. CONCLUSIONS AND FUTURE RECOMMENDATIONS

While some processing parameters studied in this research are inter-dependent, it was found that increasing the PPT over 450°F had a decreasing effect on most mechanical properties. Meanwhile, increasing the dwell from 1 min to 15 min drastically increased matrix-dominant properties such as 90° tensile strength. A slower cooling rate was the only variable that had a significant effect on polymer crystallinity but did not necessarily correlate to increased properties. The results of the thick-section PMC study demonstrated that increasing the thickness, even up to 2 in, did not create any symmetric property gradient through the cross-section. Because other microstructural properties likely had a larger impact on performance, it is recommended to use a bidirectional weave PMC in future research to reduce the effects of fiber wash. Also using a mold material that has a lower coefficient of thermal expansion, such as steel, is preferred. The level of contraction of the aluminum frame, especially after heating to higher PPTs, introduced more stress cracking and thus any increased crystallinity levels were negated. Lastly, to gain better confidence in percent crystallinity results, it is recommended to take samples from polymer-rich areas of post-processed PMCs if possible or use a different technique such as X-ray diffraction that eliminates the need to estimate fiber-weight fraction.

REFERENCES

[1] Y. Ma, Y. Yang, T. Sugahara, and H. Hamada, "A study on the failure behavior and mechanical properties of unidirectional fiber reinforced thermosetting and thermoplastic composites," *Compos B Eng*, vol. 99, pp. 162–172, 2016, doi: 10.1016/j.compositesb.2016.06.005.

[2] "$9.3 Billion Automotive Composites (Glass, Carbon, Natural) Market - Global Forecast to 2025," *Business Wire*, Jan. 22, 2021.

[3] J. Moothoo, M. Bar, and P. Ouagne, "Mechanical properties of compression moulded aggregate-reinforced thermoplastic composite scrap," *Journal of Composites Science*, vol. 5, no. 11, Nov. 2021, doi: 10.3390/jcs5110299.

[4] I. M. Daniel and O. Ishai, *Engineering Mechanics of Composite Materials*, 2nd ed. New York: Oxford University Press, 2006.

[5] H. Ning, N. Lu, A. A. Hassen, K. Chawla, M. Selim, and S. Pillay, "A review of Long fibre thermoplastic (LFT) composites," *International Materials Reviews*, vol. 65, no. 3, pp. 164–188, Apr. 2020, doi: 10.1080/09506608.2019.1585004.

[6] S. A. Mirdehghan, "Fibrous polymeric composites," *Engineered Polymeric Fibrous Materials*, pp. 1–58, Jan. 2021, doi: 10.1016/B978-0-12-824381-7.00012-3.

[7] M. Etcheverry and S. E. Barbosa, "Glass fiber reinforced polypropylene mechanical properties enhancement by adhesion improvement," *Materials*, vol. 5, no. 6, pp. 1084–1113, 2012, doi: 10.3390/ma5061084.

[8] C. H. Zweben, "Composites: Overview," *Encyclopedia of Condensed Matter Physics*, pp. 192–208, Jan. 2005, doi: 10.1016/B0-12-369401-9/00545-3.

[9] J. Markarian, "Long fibre reinforcement drives automotive market forward," *Plastics, Additives and Compounding*, vol. 7, no. 3, pp. 24–29, 2005, doi: 10.1016/S1464-391X(05)70393-7.

[10] B. Demirel, A. Yaraş, and H. ELÇİÇEK, "Crystallization Behavior of PET Materials," *Balıkesir Üniversitesi Fen Bilimleri Enstitü Dergisi*, vol. 13, pp. 26–35, Jan. 2011.

[11] P.-Y. B. Jar, R. Mulone, P. Davies, and H.-H. Kausch, "A study of the effect of forming temperature on the mechanical behaviour of carbon-fibre/peek composites," *Compos Sci Technol*, vol. 46, no. 1, pp. 7–19, 1993, doi: 10.1016/0266-3538(93)90076-S.

[12] L. Ye, K. Friedrich, J. Kästel, and Y.-W. Mai, "Consolidation of unidirectional CF/PEEK composites from commingled yarn prepreg," *Compos Sci Technol*, vol. 54, no. 4, pp. 349–358, 1995, doi: 10.1016/0266-3538(95)00061-5.

[13] J. Bernhardsson and R. Shishoo, “Effect of processing parameters on consolidation quality of GF/PP commingled yarn based composites,” *Journal of Thermoplastic Composite Materials*, vol. 13, no. 4, pp. 292–313, 2000, doi: 10.1106/X5VY-2TF0-Y3UA-D5DQ.

[14] R. H. Elleithy, M. E. Ali Mohsin, I. Ali, and S. M. Al-Zahrani, “Effect of nano - SiO <inf>2</inf> on the crystallinity and crystallization behavior (non-isothermal and isothermal) of polyethylene terephthalate (PET) nanocomposite,” in *Annual Technical Conference - ANTEC, Conference Proceedings*, 2012, pp. 2001–2007.

[15] D. LeBlanc *et al.*, “Study of processing conditions on the forming of ribbed features using randomly oriented strands thermoplastic composites,” *Journal of the American Helicopter Society*, vol. 60, no. 1, p. 011005, 2015, doi: 10.4050/JAHS.60.011005.

[16] D. Trudel-Boucher, S. Labonté, and C. Cridelich, “Long fiber thermoplastic PET-based composites: Process parameters and mechanical properties,” in *International SAMPE Technical Conference*, 2010.

[17] M. D. Wakeman, T. A. Cain, C. D. Rudd, R. Brooks, and A. C. Long, “Compression moulding of glass and polypropylene composites for optimised macro- and micro-mechanical properties - 1 commingled glass and polypropylene,” *Compos Sci Technol*, vol. 58, no. 12, pp. 1879–1898, 1998, doi: 10.1016/S0266-3538(98)00011-6.

[18] Q. Wang, X. Hu, L. Tan, and J. Gao, *Effect of hot press parameters on the consolidation quality of biaxial knitted composites from commingled yarn*, vol. 332–334. 2011. doi: 10.4028/www.scientific.net/AMR.332-334.2069.

[19] K. Fujihara, Z.-M. Huang, S. Ramakrishna, and H. Hamada, “Influence of processing conditions on bending property of continuous carbon fiber reinforced PEEK composites,” *Compos Sci Technol*, vol. 64, no. 16, pp. 2525–2534, 2004, doi: 10.1016/j.compscitech.2004.05.014.

[20] C. Gauthier, J. Chauchard, B. Chabert, J. P. Trotignon, G. Battegay, and V. Lamblin, “Crystallization and mechanical properties of a thermoplastic PET reinforced with unidirectional glass fibres,” *Plastics, Rubber and Composites Processing and Applications*, vol. 20, no. 2, pp. 77–82, 1993.

[21] N. A. Barber, *Polyethylene Terephthalate: Uses, Properties, and Degradation*. Nova Science Publishers, Inc, 2017.

[22] J. M. Charrier, *Polymeric Materials and Processing, Plastics, Elastomers, and Composites*. New York: Hanser Publishers, 1990.

[23] “Toray Cetex TC940 Technical Data Sheet,” Toray Advanced Composites.

[24] “Featured Supplier: Toray Advanced Composites,” Composites One.

[25] “Genesis Series Hydraulic Presses,” Wabash Metal Products. Inc.

[26] “ASTM D3039-17 Standard Test Method for Tensile Properties of Polymer Matrix Composite Materials.” ASTM Internation, Nov. 2017.

[27] “ASTM D695-15 Standard Test Method for Compressive Properties of Rigid Plastics.” ASTM International, Sep. 2015.

[28] “ASTM D2344-16 Standard Test Method for Short-Beam Strength of Polymer Matrix Composite Materials and Their Laminates.” ASTM International, Jul. 2016.

[29] “Maxiem 1515 Jetmachining Center,” Omax Corporation.

[30] “ASTM D3850-19 Standard Test Method for Rapid Thermal Degradation of Solid Electrical Insulating Materials By Thermogravimetric Method (TGA.” ASTM International, 2019.

[31] TA Instruments, “Thermal Analysis: Q500.”

[32] “Differential Scanning Calorimetry: Q1000,” TA Instruments.

[33] “ASTM E2160-18 Standard Test Method for Heat of Reaction of Thermally Reactive Materials by Differential Scanning Calorimetr.” ASTM International, 2018.

[34] R. L. Blaine, “Polymer Heats of Fusion.” TA Instruments, New Castle, DE.

[35] “Spider_plot - MATLAB Source Code.” 2024. Accessed: May 05, 2024. [Online]. Available: https://www.mathworks.com/matlabcentral/fileexchange/59561-spider_plot?s_tid=srchtitle

[36] D. Xiang, E. Harkin-Jones, and D. Linton, “Effect of cooling rate on the properties of high density polyethylene/multi-walled carbon nanotube composites,” in *AIP Conference Proceedings*, 2015. doi: 10.1063/1.4918440.

[37] C. Doetkott, “ANOVA - SAS Source Code.” 2024.

APPENDIX

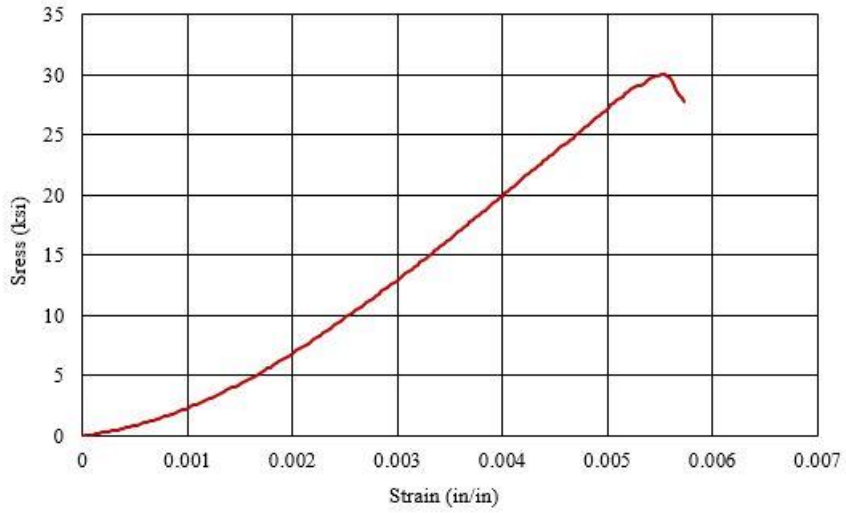

Figure A1. Stress-strain curve of Set 1 470°F 0° compression specimen

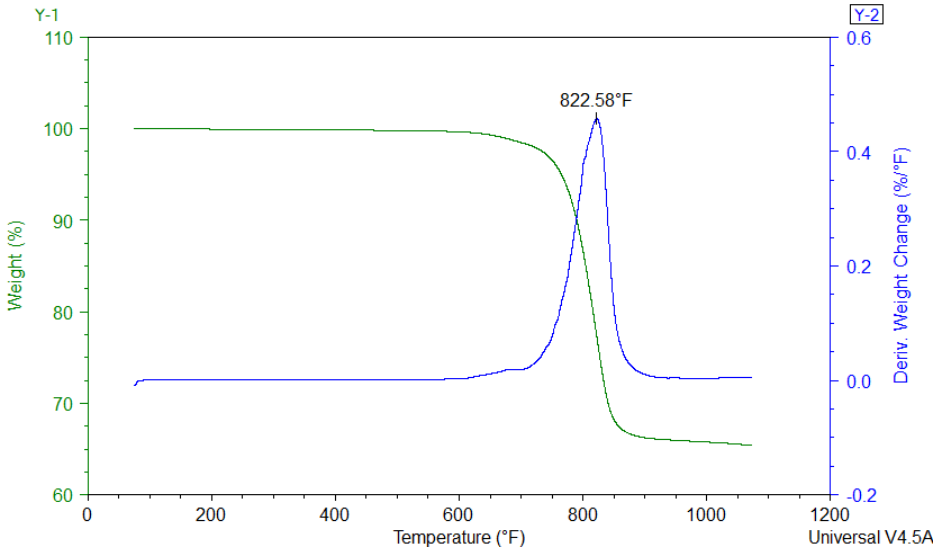

Figure A2. TGA graph showing degradation temperature of Toray PET

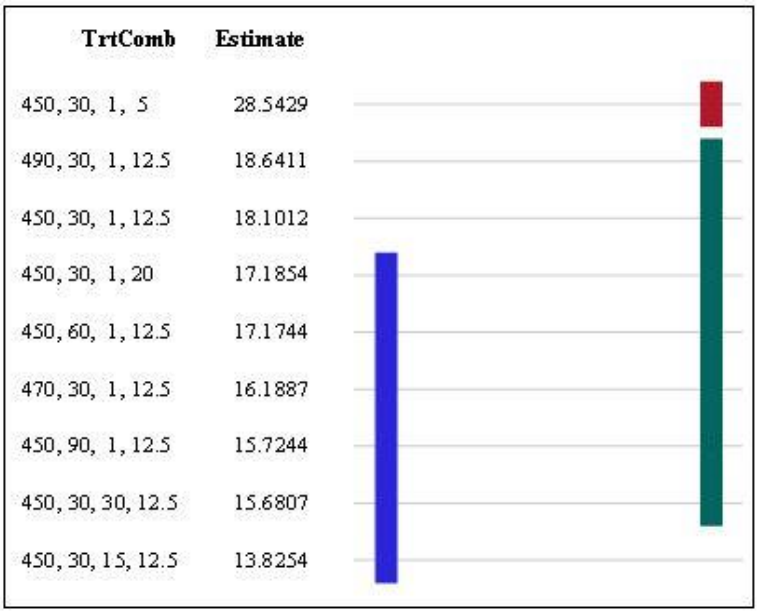

Figure A3. Sets 1-4 Duncan grouping for percent crystallinity [37]

Note: Means covered by the same bar are not significantly different at 95% confidence

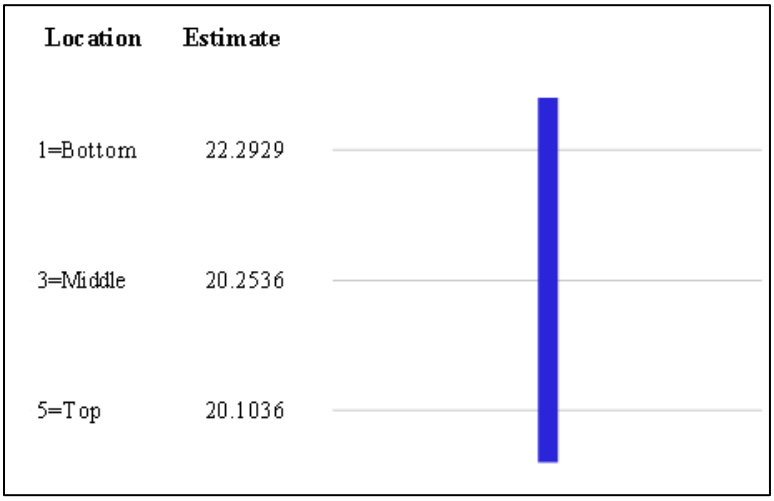

Figure A4. Set 6 Duncan grouping for percent crystallinity

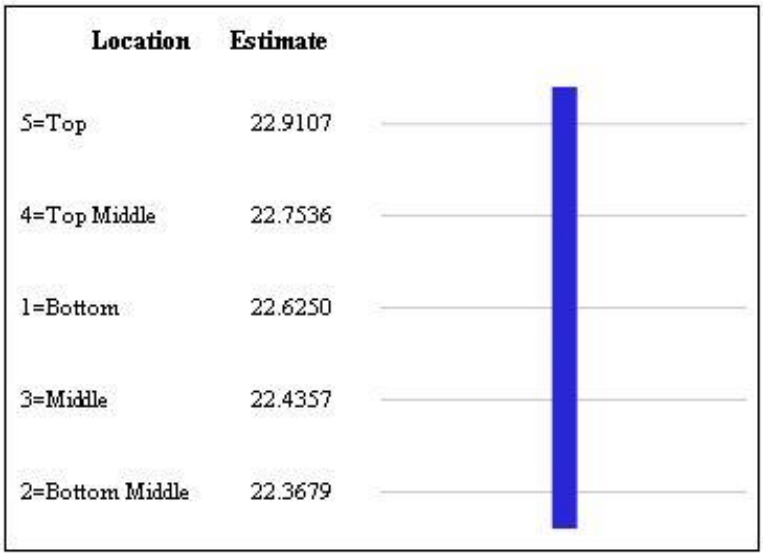

Figure A5. Set 5 Duncan grouping for percent crystallinity

a)

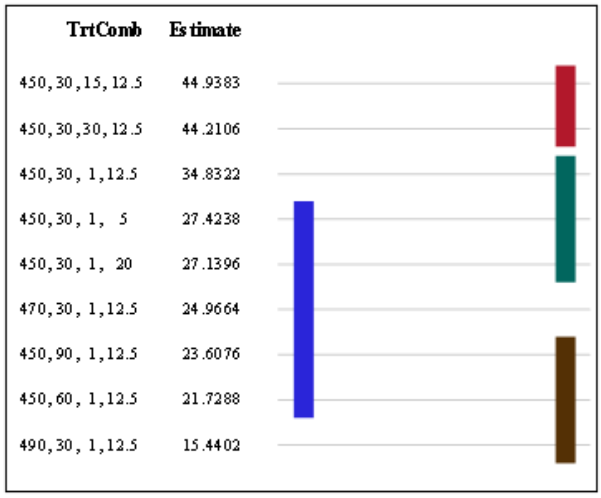

b)

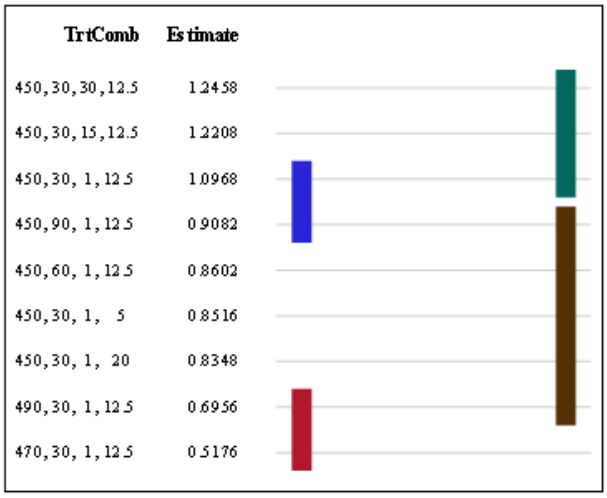

Figure A6. Sets 1-4 Duncan grouping for a) 0° CS (ksi) and b) 0° CM (ksi)

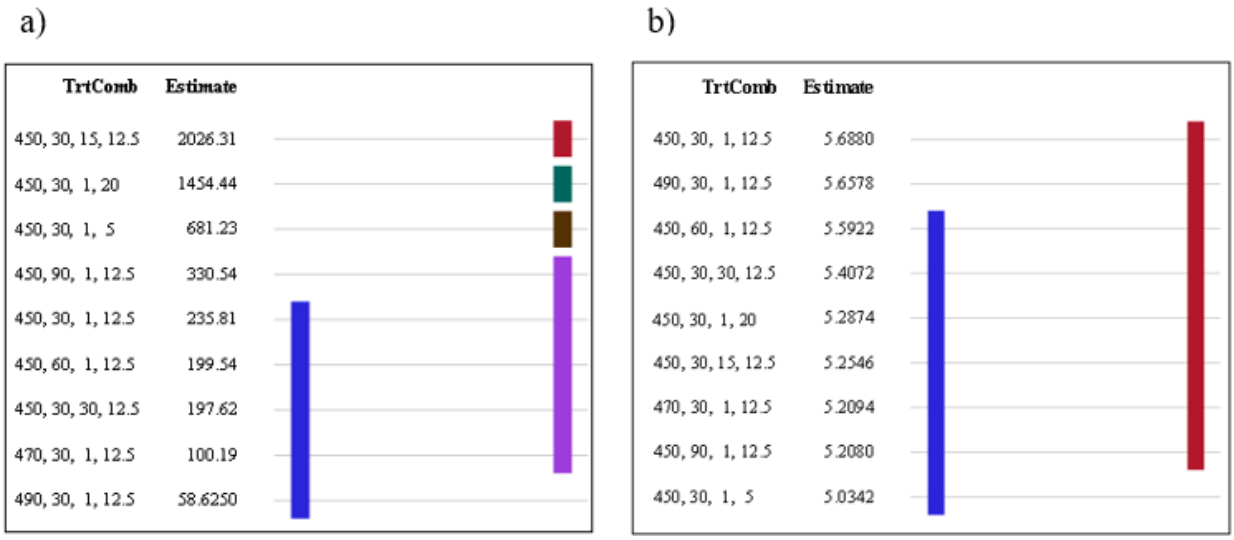

Figure A7. Sets 1-4 Duncan grouping for a) 90° TS (psi) and b) 0° TM (Msi)

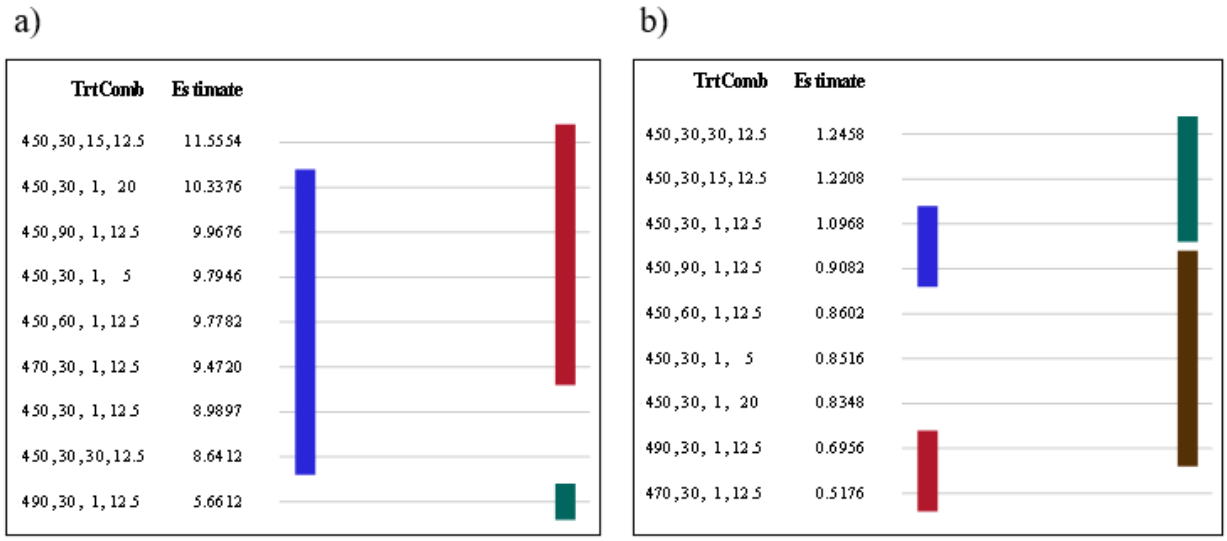

Figure A8. Sets 1-4 Duncan grouping for a) 90° CS (ksi) and b) 90° CM (Msi)

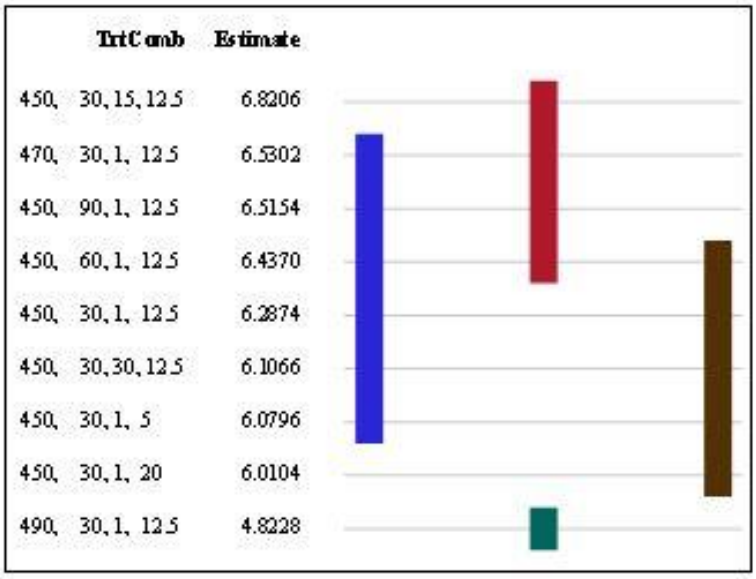

Figure A9. Sets 1-4 Duncan grouping for ILSS (ksi)

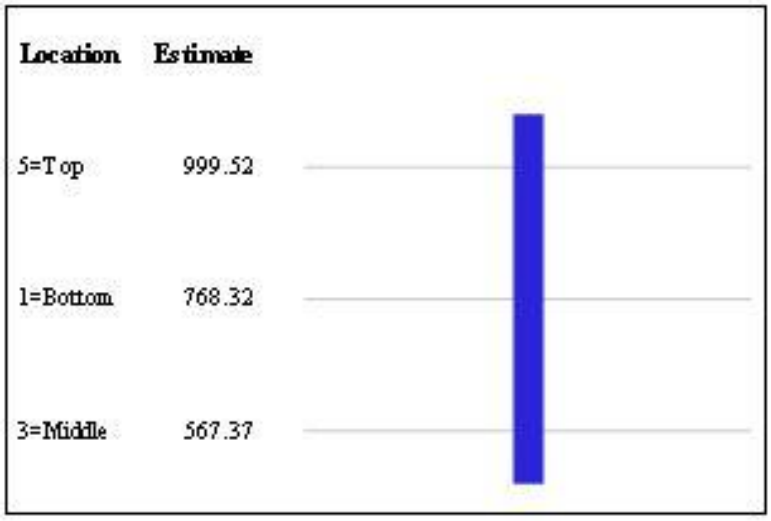

Figure A10. Set 5 Duncan grouping for 90° TS (psi)

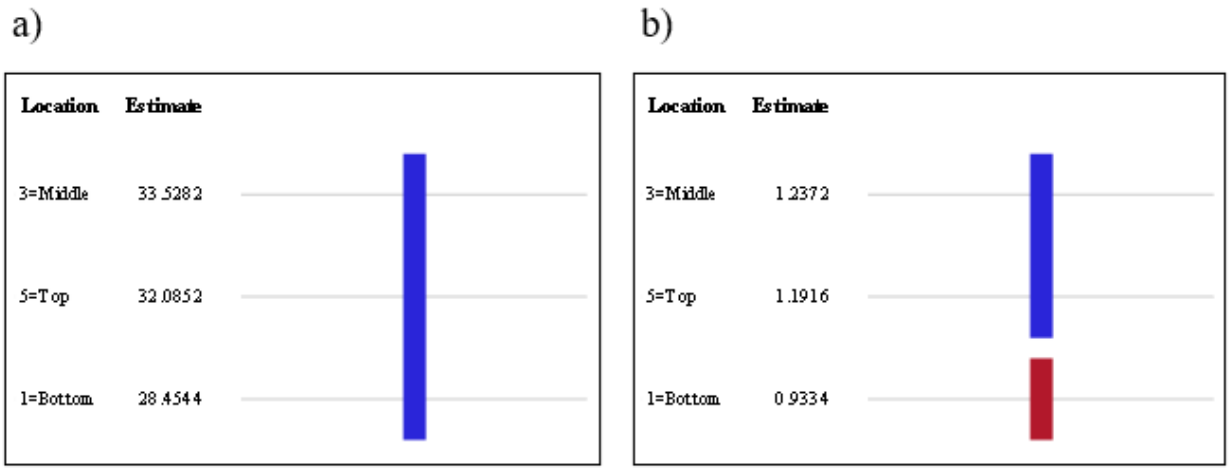

Figure A11. Set 5 Duncan grouping for a) 0° CS (ksi) and b) 0° CM (Msi)

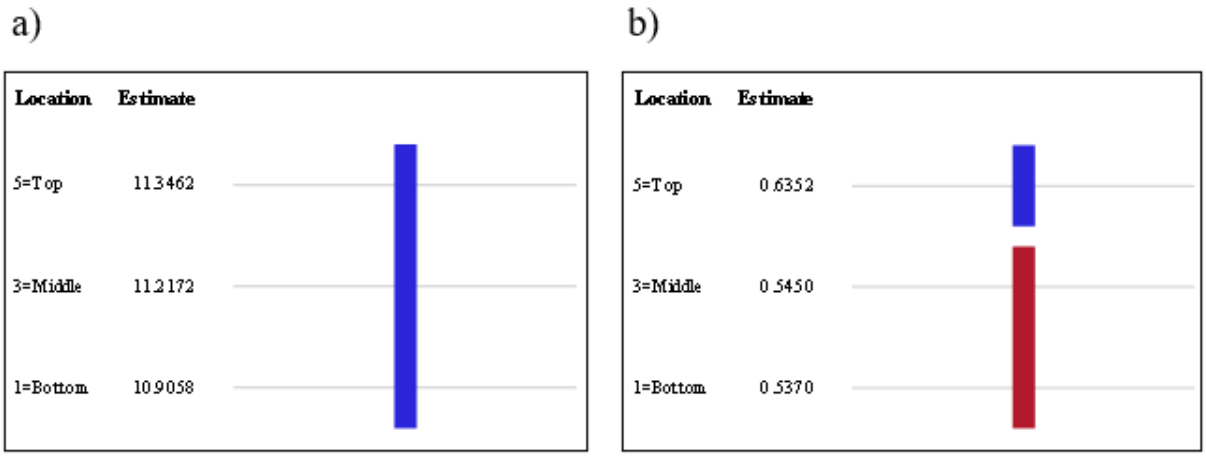

Figure A12. Set 5 Duncan grouping for a) 90° CS (ksi) and b) 90° CM (Msi)

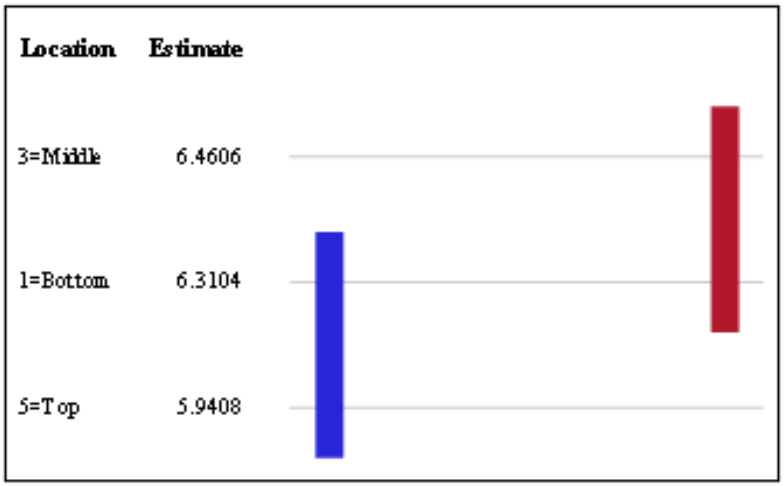

Figure A13. Set 5 Duncan grouping for ILSS (ksi)

a)

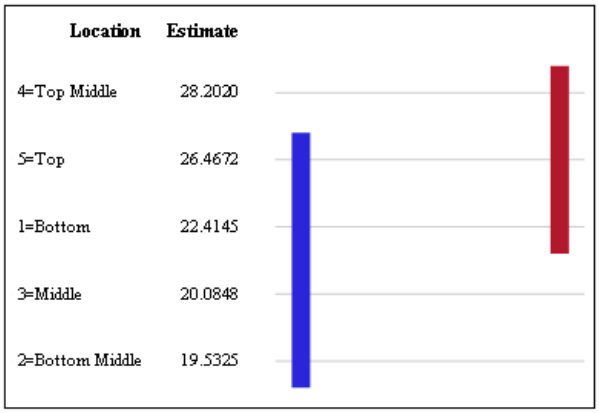

b)

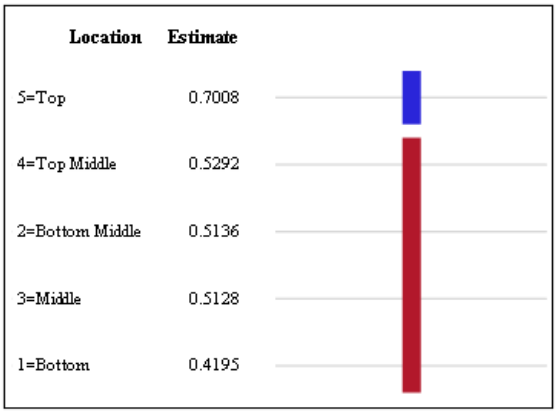

Figure A14. Set 6 Duncan grouping for a) 0° CS (ksi) and b) 0° CM (Msi)

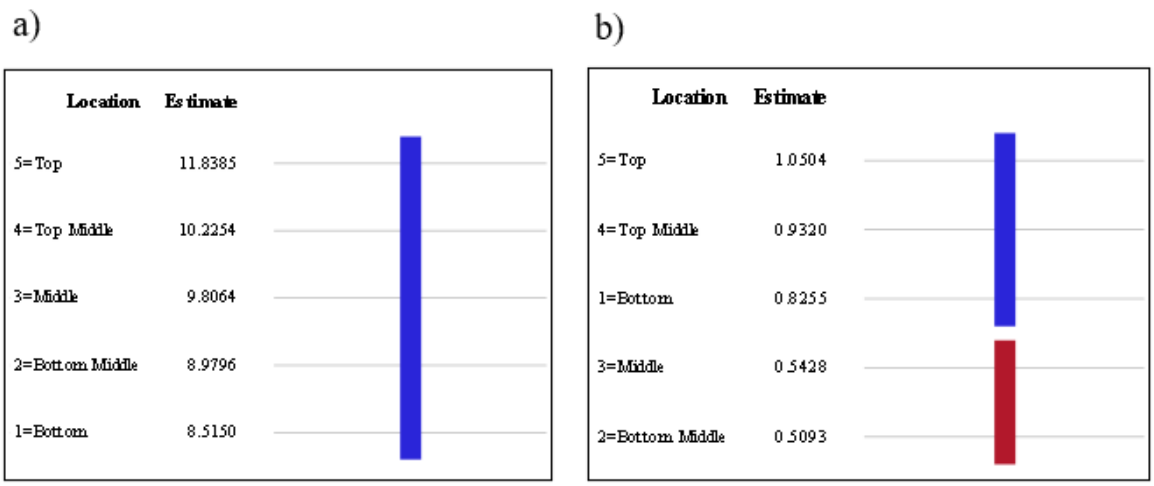

Figure A15. Set 6 Duncan grouping for a) 90° CS (ksi) and b) 90° CM (Msi)

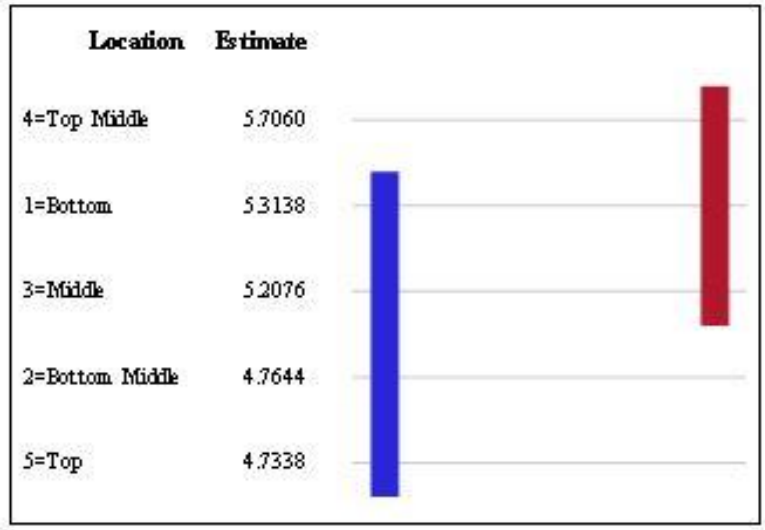

Figure A16. Set 6 Duncan grouping for ILSS (ksi)